The Yang Research Group
Precise Synthesis Lab at Tongji University

Group Topic

Betley Group's Work

Reporter: Dong-Song Zheng

Date: 2025.10.17

CONTENTS
目录

Theodore A. Betley

Professional experience

2008 - present Professor, Harvard University;

2007 - 2008 Postdoctoral Fellow, Massachusetts Institute of Technology (MIT); Advisor: Prof. Daniel G. Nocera. (solar energy conversion and storage; PCET)

2002 - 2007 Ph.D., California Institute of Technology; Advisor: Prof. Jonas C. Peters. ((bio)inorganic, organometallic, electrocatalysis, photocatalysis (PCET)).

1998 - 2002 B.S., University of Michigan; Major: Chemical Engineering.

Research

(1) Synthetic inorganic chemistry.

(2) First-row transition elements

(3) Organometallic catalysis and small molecule activation

(4) C–H bond functionalization.

(1) 同质异能位移

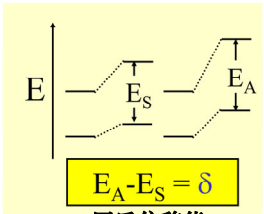

同质位移能

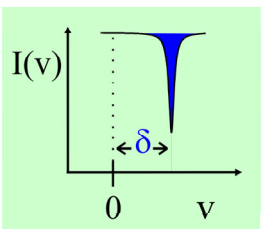

核电荷分布程球对称

(2) 四极分裂

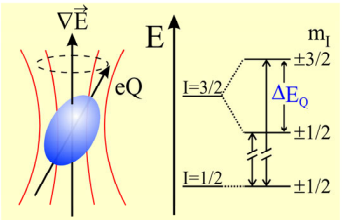

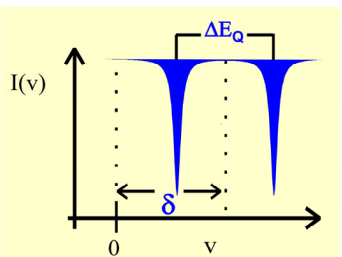

核电荷分布偏离球对称

(2) 磁超精细分裂

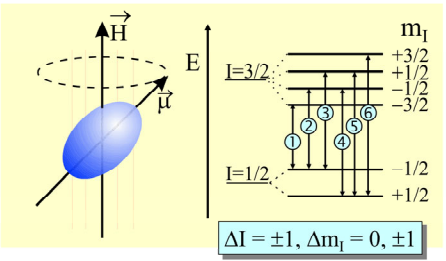

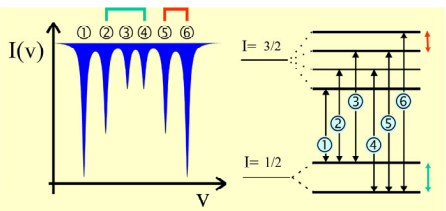

原子核处于磁场

氧化态	自旋态	同质异能位移 (δ, mm/s)
Fe(I)	低自旋 (S=2)	0.5 – 0.8
Fe(II)	高自旋 (S=2)	0.7 - 1.3
Fe(II)	低自旋 (S=0)	0.3 - 0.5
Fe(III)	高自旋 (S=5/2)	0.2 - 0.5
Fe(III)	低自旋 (S=1/2)	0.0 - 0.3
Fe(IV)	高自旋 (S=2)	0.2 - 0.4
Fe(II)	低自旋 (S=1)	-0.1 - 0.1
Fe(V)	低自旋 (S=1/2)	-0.5 - -0.2
Fe(VI)	低自旋 (S=0)	-0.8 - -0.9

配体轨道能级高于金属d轨道

J|A|C|S
ARTICLES

Published on Web 09/15/2009

Unusual Electronic Structure of First Row Transition Metal Complexes Featuring Redox-Active Dipyrromethane Ligands

Evan R. King and Theodore A. Betley*

Department of Chemistry and Chemical Biology, Harvard University, 12 Oxford Street, 306E Mallinckrodt, Cambridge, Massachusetts 02138

Received May 16, 2009; E-mail: betley@chemistry.harvard.edu

Abstract: Transition metal complexes (Mn → Zn) of the dipyrromethane ligand, 1,9-dimesityl-5,5-dimethyldipyrromethane (dpm), have been prepared. Arylation of the dpm ligand α to the pyrrolic nitrogen donors limits the accessibility of the pyrrole π-electrons for transition metal coordination, instead forcing η^1,η^1 coordination to the divalent metal series as revealed by X-ray diffraction studies. Structural and magnetic characterization (SQUID, EPR) of the bis-pyridine adducts of $(dpm)Mn^{II}(py)_2$, $(dpm)Fe^{II}(py)_2$, and $(dpm)Co^{II}(py)_2$ reveal each divalent ion to be high-spin and pseudotetrahedral in the solid state, whereas the $(dpm)Ni^{II}(py)_2$ is low-spin and adopts a square-planar geometry. Differential pulse voltammetry on the

J. Am. Chem. Soc. **2009**, *131*, 14374.

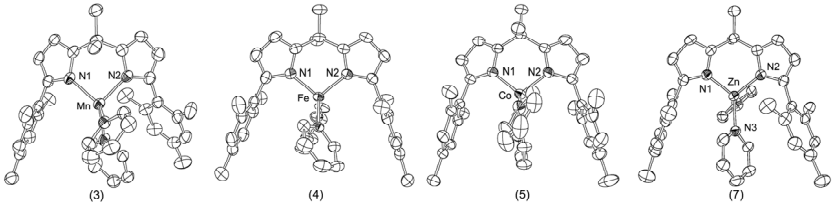

Mn (3), Fe (4)
Co (5), Ni (6)
Zn (7)

[(dpm)CoCl(THF)][Li(THF)$_2$] (**8**)
(dpm)Fe^{II}(bpy) (**9**)

Figure 1. Solid-state molecular structures for complexes **3**, **4**, **5**, and **7** with the thermal ellipsoids set at the 50% probability level (hydrogen atoms and minor structural disorder in **3** and **4** are omitted for clarity).

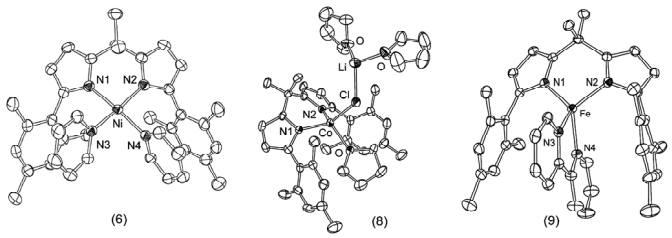

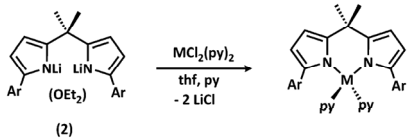

1. **配体电子还原金属**
2. **自旋态互变异构**
3. **无分子内氧化还原**（金属保持二价，配体完全还原）

Figure 2. Solid-state molecular structures for complexes **6**, **8**, and **9** with the thermal ellipsoids set at the 50% probability level (hydrogen atoms, one solvent molecule for **6**, and two solvent molecules for **9** are omitted for clarity). The Li^+ in **8** is coordinated to an adjacent molecule's pyrrole ring.

Table 1. Magnetic and Spectral Properties of Complexes **3**, **4**, **5**, and **9**

complex	S	μ_{eff} (BM)	λ/nm (ε/M$^{-1}\cdot$cm^{-1})	δ (mm/s)	ΔE_q (mm/s)
(dpm)Mn(py)$_2$ (**3**)	$^5/_2$	5.97,[a] 6.1(1)[b]	–	–	–
(dpm)Fe(py)$_2$ (**4**)	2	5.00,[a] 5.2(1)[b]	420 (1500), 1359 (70), 1675 (50) (sh)	0.80 0.86	3.46 2.63
(dpm)Fe(bpy) (**9**)	2	5.1(1)[b]	535 (410), 585 (620), 613 (870), 1125 (110), 1260 (105) (sh)	0.72	3.00
(dpm)Co(py)$_2$ (**5**)	$^3/_2$	4.20,[a] 4.5(1)[b]	395 (1100)	–	–
(dpm)Ni(py)$_2$ (**6**)	0	–	503 (190)	–	–

[a] Average moment over T range of 200−300 K from SQUID. [b] Room temperature (295 K) moment in solution by Evans's method.

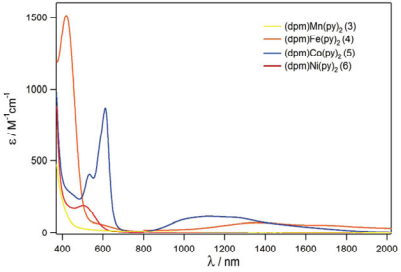

Figure 3. UV/vis/NIR molar absorptivity spectra of **3**, **4**, **5**, and **6**. Spectra were taken in dichloromethane, molar absorptivities are based on measurements at four concentrations.

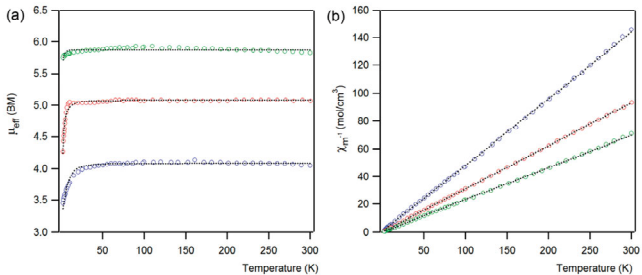

Figure 4. (a) SQUID magnetization data for complexes **3** (green ○), **4** (red ○), and **5** (blue ○) shown as a plot of μ_{eff} (BM) versus T (K) and (b) as a plot of χ_m^{-1} (mol/cm^3) versus T (K). Dotted lines are the simulations of each data set.[19]

d-d跃迁

磁化率倒数（χ_m^{-1}）与温度（T）成直线，排除自旋态互变异构

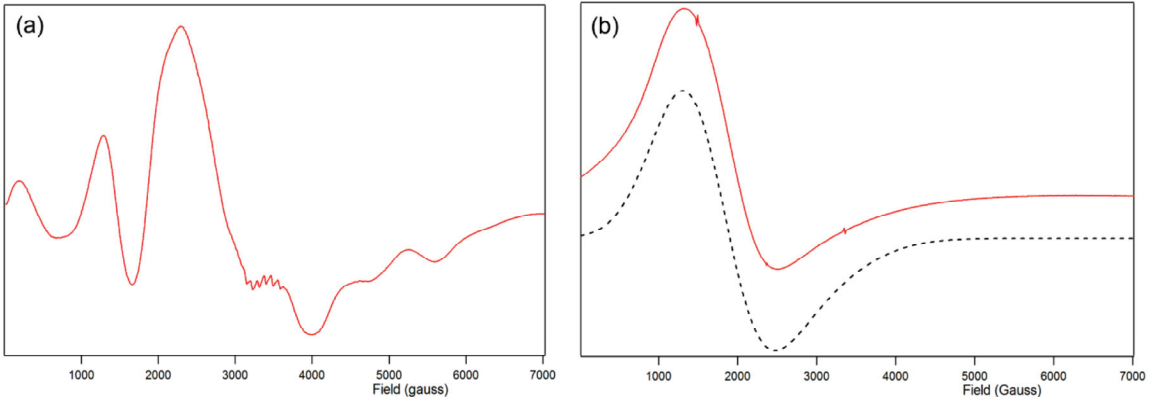

Figure 5. Powder EPR spectrum of (a) (dpm)Mn(py)$_2$ (**3**) and (b) (dpm)Co(py)$_2$ (**5**) (dotted line is data simulation: $g_\perp$ 2.02, $g_\parallel$ 2.31; $A_\perp$ 0, $A_\parallel$ 0.0112 cm^{-1}; D 7.855 cm^{-1}, E/D 0) (77 K, X-band, 9.397 GHz).

配合物	EPR观测结果	支持的结论	排除的竞争场景
(dpm)Mn(py)$_2$ (3)	复杂的多线谱	**1. 确认高自旋Mn(II)中心。** **2. 自旋密度定域在Mn上。**	**Scenario 1:** 排除了配体被氧化形成有机自由基的可能性。
(dpm)Co(py)$_2$ (5)	1. g≈3.48的信号。 2. 信号持续到室温。	**1. 确认高自旋Co(II)中心。** **2. 表明存在单一、稳定的高自旋基态。**	**Scenario 2:** 排除了自旋态互变异构，因为信号在宽温区内稳定存在。

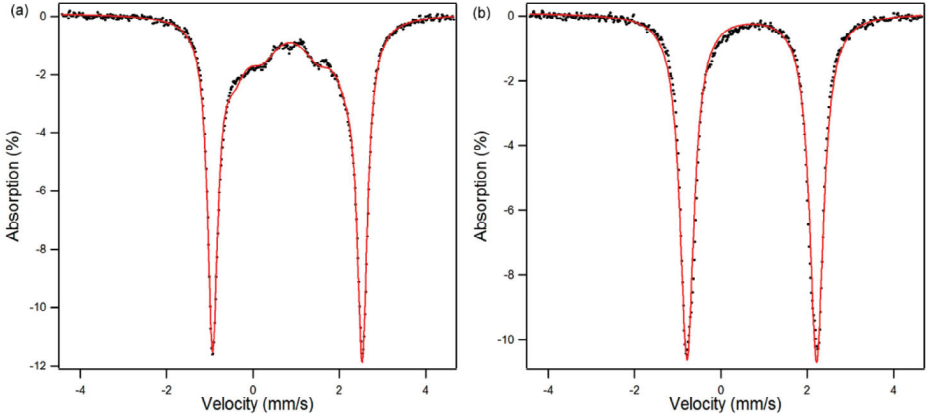

Figure 6. Zero-field Mössbauer spectrum of (a) (dpm)Fe(py)$_2$ (**4**) and (b) (dpm)Fe(bpy) (**9**) at 4.2 K.

Fe (II) 低s电子密度导致跃迁能增大，在穆斯堡尔谱上表现为更大的异构位移δ值。

氧化态与自旋态	典型异构位移范围 (δ, mm/s)	文章中的数值	结论
高自旋 Fe(III)	0.2 - 0.5	**0.72 - 0.86**	**完全不符**
高自旋 Fe(II)	**0.7 - 1.3**	**0.72 - 0.86**	**完美吻合**

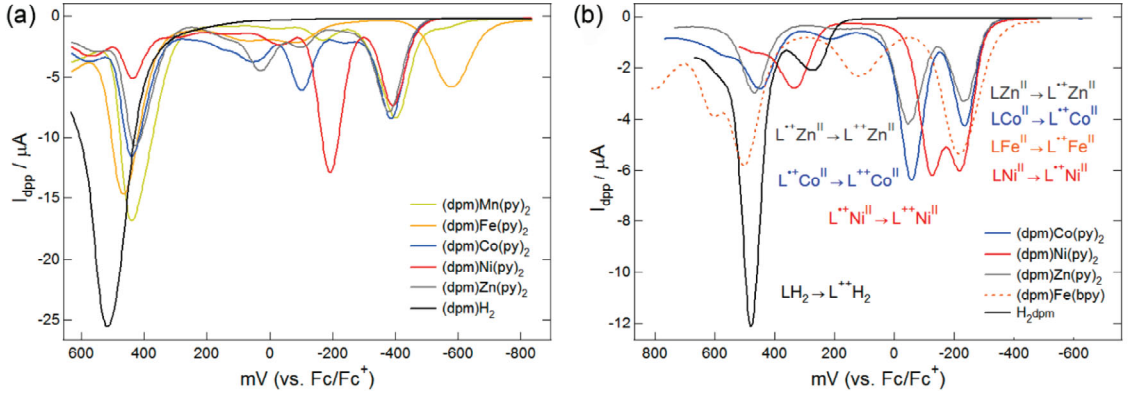

Figure 7. Differential pulse voltammograms of (a) solutions in THF of 10^{-4} M (dpm)M, where M = $Mn(py)_2$ (**3**), $Fe(py)_2$ (**4**), $Co(py)_2$ (**5**), $Ni(py)_2$ (**6**), $Zn(py)_2$ (**7**), H_2 (**1**); Bu_4NPF_6 (0.3 M); scan rate 20 mV/s on glassy C electrode), and (b) solutions in acetonitrile of 10^{-4} M (dpm)M, where M = $Co(py)_2$ (**5**), $Ni(py)_2$ (**6**), $Zn(py)_2$ (**7**), Fe(bpy) (**9**), H_2 (**1**); Bu_4NPF_6 (0.1 M); scan rate 20 mV/s on Pt electrode.

差分脉冲伏安法 (DPV): (1) 氧化电位与金属种类无关，说明氧化过程是配体中心的，而非金属中心。(2) 自由配体 $dpmH_2$ 的氧化电位比金属配合物高约 700 mV，说明金属配位显著降低了配体的氧化势。

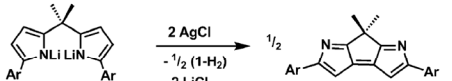

核心突破点是首次分离出高自旋Fe(III)-亚胺自由基物种，这颠覆了传统Fe(IV)=NR的认知。

JACS
JOURNAL OF THE AMERICAN CHEMICAL SOCIETY
ARTICLE
pubs.acs.org/JACS

Catalytic C−H Bond Amination from High-Spin Iron Imido Complexes

Evan R. King, Elisabeth T. Hennessy, and Theodore A. Betley*

Department of Chemistry and Chemical Biology, Harvard University, 12 Oxford Street, Cambridge, Massachusetts 02138, United States

Supporting Information

ABSTRACT: Dipyrromethene ligand scaffolds were synthesized bearing large aryl (2,4,6-$Ph_3C_6H_2$, abbreviated Ar) or alkyl (^{t}Bu, adamantyl) flanking groups to afford three new disubstituted ligands (^{R}L, 1,9-R_2-5-mesityldipyrromethene, R = aryl, alkyl). While high-spin ($S = 2$), four-coordinate iron complexes of the type (^{R}L)FeCl(solv) were obtained with the alkyl-substituted ligand varieties (for R = ^{t}Bu, Ad and solv = THF, OEt_2), use of the sterically encumbered aryl-substituted ligand precluded binding of solvent and cleanly afforded a high-spin ($S = 2$), three-coordinate complex of the type (^{Ar}L)FeCl. Reaction of (^{Ad}L)FeCl(OEt_2) with alkyl azides resulted in the catalytic amination of C−H bonds or olefin aziridination at room temperature. Using a 5% catalyst loading, 12 turnovers were

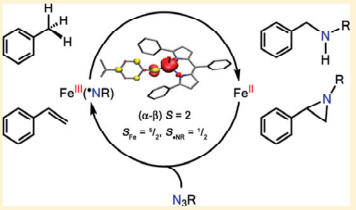

J. Am. Chem. Soc. **2011**, *133*, 4917.

Scheme 1. Ligand and Metal Complex Syntheses

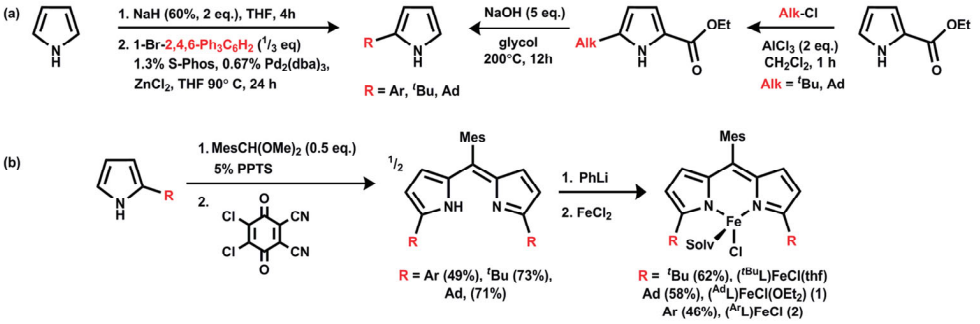

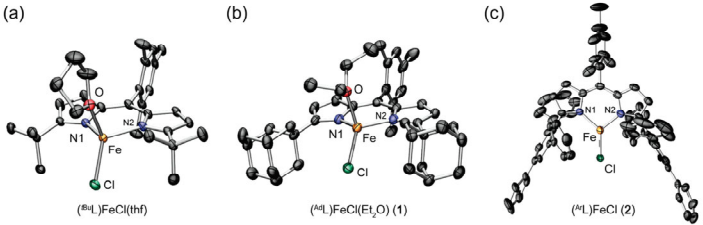

Scheme 3. Synthesis of the Bimolecularly Coupled Fe^{III} Imido Precursor 3 and the Terminal Imido Complex 4 with a Delocalized Imido-Based Radical, $Fe^{III}(^{\bullet}NAr)$, and Their Subsequent Reactivity with C−H Bonds

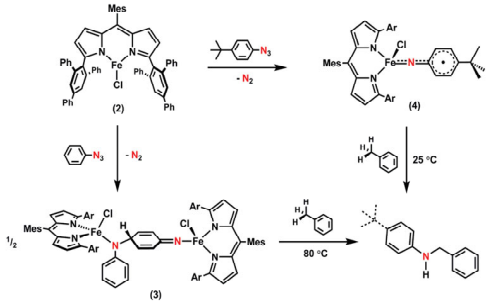

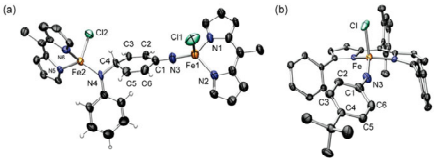

Figure 2. Solid-state core molecular structures for (a) 3 and (b) 4. Ligand aryl substituents, hydrogen atoms, and solvent molecules are omitted for clarity. Bond lengths (Å) are as follows. For 3: Fe1−N3, 1.810(2); Fe1−Cl1, 2.207(1); C1−N3, 1.376(3); C1−C2, 1.467(4); C2−C3, 1.378(3); C3−C4, 1.490(4); C4−C5, 1.389(4); C5−C6, 1.331(3); C6−C1, 1.462(4); N4−C4, 1.484(3); Fe2−Cl2, 2.228(1); Fe2−N4, 1.886(2). For 4: Fe−Cl, 2.210(1); Fe−N3, 1.768(2); N3−C1, 1.331(2); C1−C2, 1.423(3); C2−C3, 1.372(3); C3−C4, 1.406(3); C4−C5, 1.405(3); C5−C6, 1.378(3); C6−C1, 1.414(3).

络合物4：超长的Fe-N亚胺键 (1.768 Å)，比已知Fe(IV)=NR键长约0.1 Å。亚胺芳环的键长显示出自由基离域的特征。

Table 1. Spectral and Magnetic Properties of Complexes 1−4 $\varepsilon > 20{,}000\ M^{-1}\ cm^{-1}$

complex	μ_{eff} (μ_B)	S	λ/nm (ε/M^{-1} cm^{-1})	δ (mm/s)[b]	$\lvert\Delta E_Q\rvert$ (mm/s)[b]
(^{tbu}L)FeCl(thf)	5.2(2)	2	497 (40 000)[a]		
(^{Ad}L)FeCl(OEt$_2$) (**1**)	5.1(1)	2	494 (59 000)[a]	0.98	3.70
(^{Ar}L)FeCl (**2**)	5.1(2)	2	554 (26 000)	0.68	0.68
[(^{Ar}L)FeCl]$_2$(μ-N(Ph)(C$_6$H$_5$)N) (**3**)	7.8(2)	5/2, 5/2	551 (27 000)	0.33	2.15
(^{Ar}L)FeCl(NC$_6$H$_4$-*p*-^{t}Bu) (**4**)	5.3(1)	2	553 (26 000)	0.29	2.29

[a] UV/vis reported for pyridine adduct. [b] Recorded at 105 K.

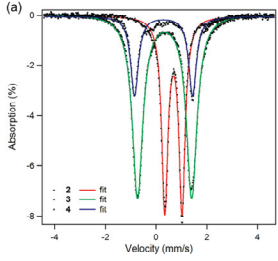

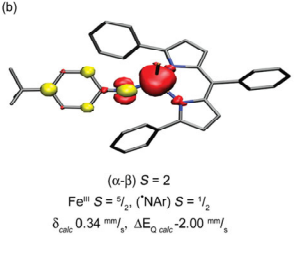

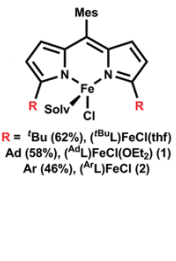

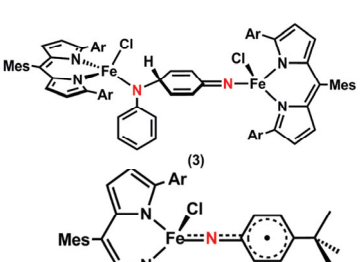

Figure 3. Terminal imido radical complex **4** exhibiting Mössbauer metrical parameters nearly identical with those of the bimolecularly coupled diferric **3**, illustrated in (a) by the zero-field 100 K ^{57}Fe Mössbauer spectral data, presented as black dots with spectral fits as solid lines (δ, $|\Delta E_Q|$ (mm/s)): Fe^{III} **2** (red) 0.68, 0.68; $(Fe^{III})_2$ **3** (green) 0.33, 2.15; Fe^{III}(•NAr) **4** (blue) 0.29, 2.29) and antiferromagnetic coupling between the high-spin Fe^{III} ion with the terminal imido radical in **4**, illustrated in (b) by the calculated spin density population ($\alpha - \beta$) for **4** ($S = 2$) by DFT (B3LYP/TZVP, SV(P); ORCA 2.7[58]).

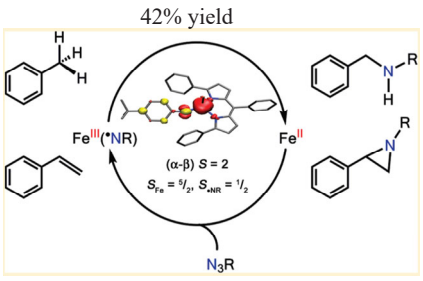

Scheme 2. Proposed Catalytic Cycle for the Amination of C−H Bonds by Reaction of 1 with Organic Azides

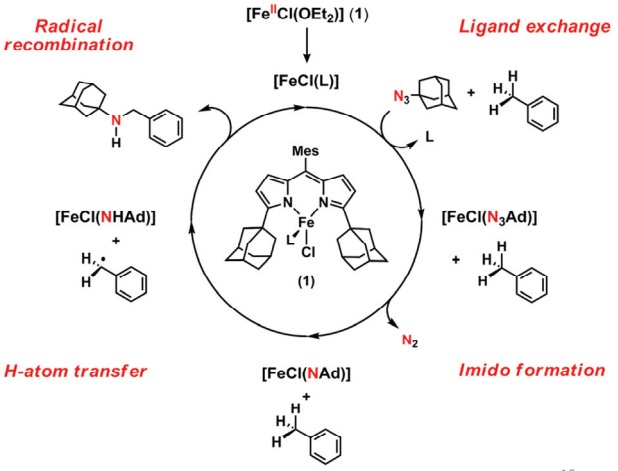

Complex N-Heterocycle Synthesis via Iron-Catalyzed, Direct C–H Bond Amination

Elisabeth T. Hennessy and Theodore A. Betley*

Science **2013**, *340,* 591.

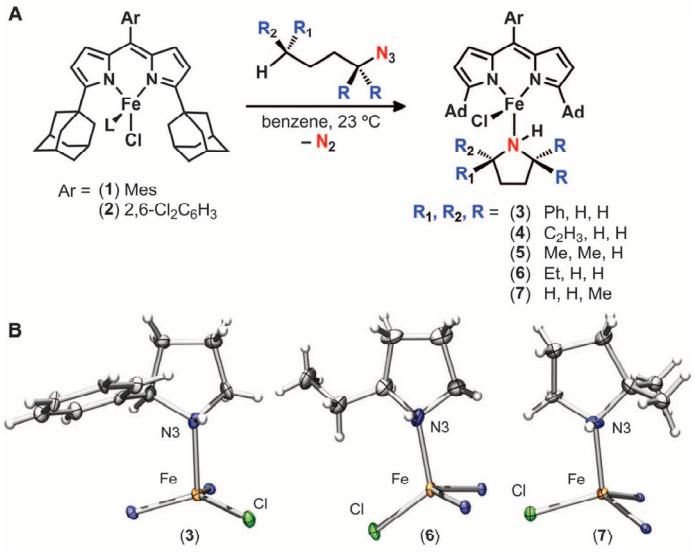

单核金属络合物 (Fe)

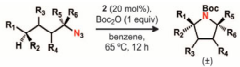

Entry	Azide	Pyrrolidine	Yield (%)*	Entry	Azide	Pyrrolidine	Yield (%)*
1			98[†§] (PG = Fmoc) 93[†§] 57[†§] (PG = Boc)	10			66 1.5:1.0 dr
2			72[†§]	11			70
3			60[§] 49[†§]	12			98
4			19[†§]	13			75[‡] 93% ee
5			17[†§]	14			84 1.1:1.0 dr
6			11	15			67
7			47	16			73 2.1:1.0 dr
8			68[‡]	17			58 5.5:1.5: 1.0:0.08 dr
9			60 3.9:1.0 dr	18			14 (PG = Boc) 78[†] (PG = Fmoc)

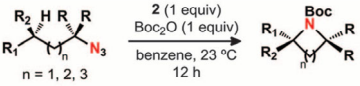

Entry	Azide	Product(s)	Conv. (%)*†
1			45
2			82
3			52 (1.0:0.9)
4			47 (1.0:1.5)
5			47 (1.0:1.5)

* Yields determined by ^{1}H NMR using ferrocene or trimethoxybenzene as internal standards. † Ratios determined by integration of GC/MS peaks.

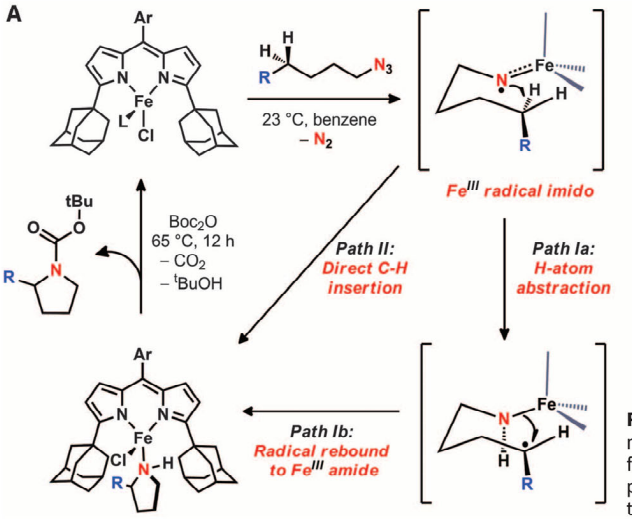

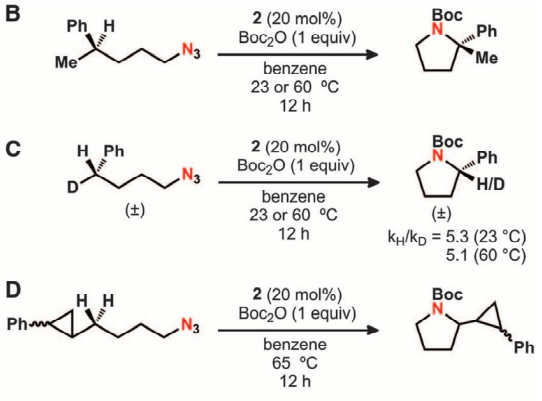

Fig. 2. Mechanistic studies. (**A**) Proposed mechanistic pathways for intramolecular C–H amination of linear alkyl azides with Fe catalyst **1** or **2** to form N-heterocycles. Pyrrolidine formation is depicted, although azetidine and piperidine products are also accessible. (**B** to **D**) Substrates designed to probe the mechanism of C–H functionalization and distinguish between paths I and II.

JACS
JOURNAL OF THE AMERICAN CHEMICAL SOCIETY
Article
pubs.acs.org/JACS

Characterization of Iron-Imido Species Relevant for *N*-Group Transfer Chemistry

Diana A. Iovan and Theodore A. Betley*

Department of Chemistry and Chemical Biology, Harvard University, 12 Oxford Street, Cambridge, Massachusetts 02138, United States

Supporting Information

ABSTRACT: A sterically accessible *tert*-butyl-substituted dipyrrinato di-iron(II) complex $[(^{tBu}L)FeCl]_2$ possessing two bridging chloride atoms was synthesized from the previously reported solvento adduct. Upon treatment with aryl azides, the formation of high-spin Fe^{III} species was confirmed by ^{57}Fe Mössbauer spectroscopy. Crystallographic characterization revealed two possible oxidation products: (1) a terminal iron iminyl from aryl azides bearing *ortho* isopropyl substituents, $(^{tBu}L)FeCl(^{\bullet}NC_6H_3\text{-}2,6\text{-}^{i}Pr_2)$; or (2) a bridging di-iron imido arising from reaction with 3,5-bis(trifluoromethyl)aryl azide, $[(^{tBu}L)FeCl]_2(\mu\text{-}NC_6H_3\text{-}3,5\text{-}(CF_3)_2)$. Similar to the previously reported $(^{Ar}L)FeCl(^{\bullet}NC_6H_4\text{-}4\text{-}^{t}Bu)$, the monomeric iron imido is best described as a high spin Fe^{III} antiferromagneti-

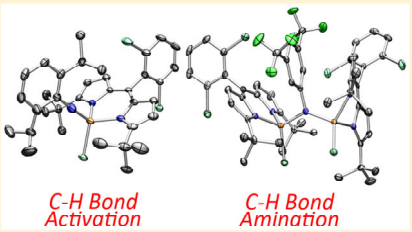

Scheme 1

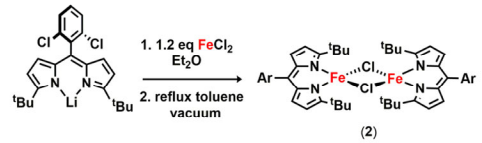

Scheme 3

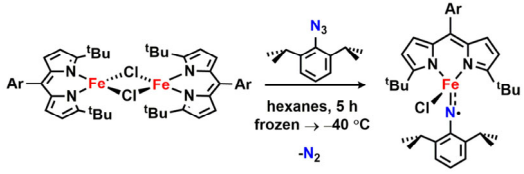

(^{t}BuL)FeCl(•NC$_6$H$_3$-2,6-iPr_2) **(3)**

δ = 0.37 mm/s

Fe–N键较长（1.768 Å）

Scheme 4

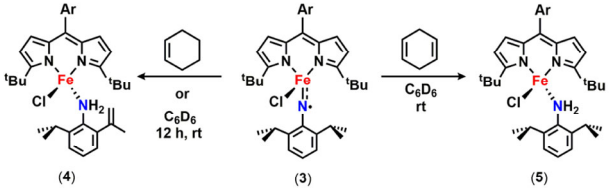

Scheme 5

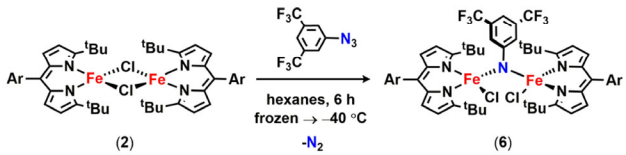

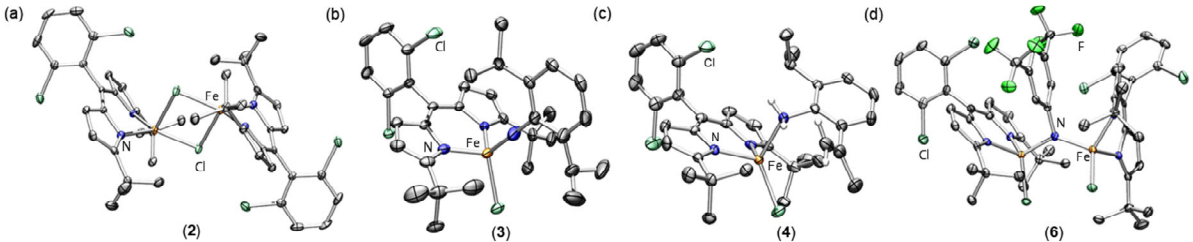

Figure 2. Solid-state molecular structures for (a) $[(^{tBu}L)FeCl]_2$ (**2**), (b) $(^{tBu}L)FeCl(^{\bullet}NC_6H_3\text{-}2,6\text{-}^{i}Pr_2)$ (**3**), (c) $(^{tBu}L)FeCl(H_2NC_6H_3\text{-}2\text{-}^{i}Pr_2\text{-}6\text{-}C(CH_2)(CH_3))$ (**4**), and (d) $[(^{tBu}L)FeCl]_2(\mu\text{-}NC_6H_3\text{-}3,5\text{-}(CF_3)_2)$ (**6**) with thermal ellipsoids at 50% probability level. Color scheme: Fe, orange; N, blue; Cl, aquamarine; F, green. Hydrogens, solvent molecules, and disordered isopropyl group in **3** are omitted for clarity.

Scheme 6

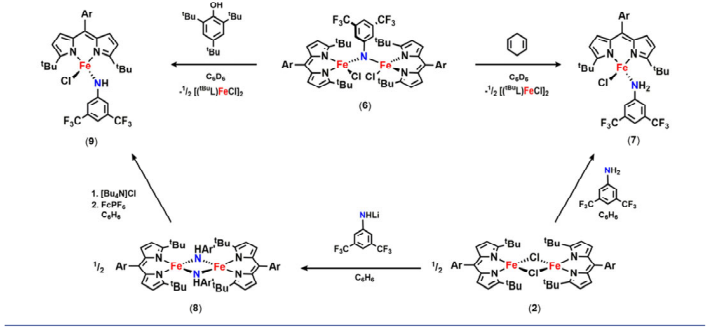

Figure 5. Solid-state molecular structures for (a) [(^{tBu}L)Fe(NHAr')]$_2$ (**8**), (b) (^{tBu}L)FeCl(NHAr') (**9**), and (c) (^{tBu}L)Fe(NHAr')$_2$ (**11**) with thermal ellipsoids at 50% probability level. Color scheme: Fe, orange; N, blue; Cl, aquamarine; F, green. Hydrogens, solvent molecules, and disordered trifluoromethyl groups in **11** are omitted for clarity; Ar' = 3,5-bis(trifluoromethyl)phenyl. (d) Mulliken spin density plot calculated[65] for 9, illustrating 7.72% spin density on the nitrogen atom.

Scheme 8

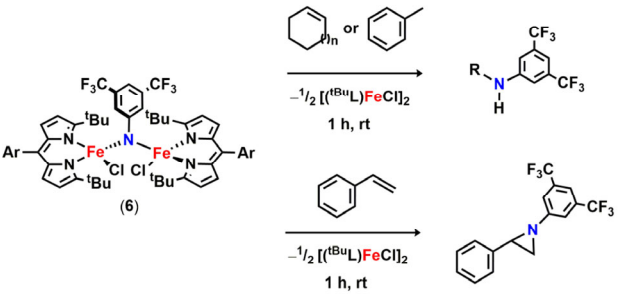

Scheme 9

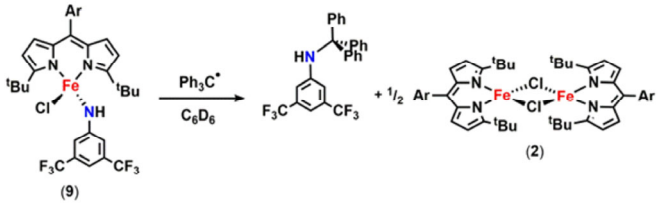

Scheme 10

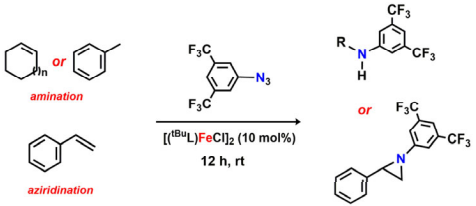

Substrate	Product	Yield (%)
	NHAr	76[a]
	ArHN	35[a]
	ArHN, ArHN	85[a]
	NHAr	21[b]
	NAr	92[c]

JACS
JOURNAL OF THE AMERICAN CHEMICAL SOCIETY
Article
pubs.acs.org/JACS

High-Spin Iron Imido Complexes Competent for C–H Bond Amination

Matthew J. T. Wilding, Diana A. Iovan, and Theodore A. Betley*

Department of Chemistry and Chemical Biology, Harvard University, 12 Oxford Street, Cambridge, Massachusetts 02138, United States

Supporting Information

ABSTRACT: Reduction of previously reported $(^{Ar}L)FeCl$ with potassium graphite furnished a low-spin ($S = 1/2$) iron complex $(^{Ar}L)Fe$ which features an intramolecular η^6-arene interaction and can be utilized as an Fe^I synthon (^{Ar}L = 5-mesityl-1,9-(2,4,6-$Ph_3C_6H_2$)dipyrrin). Treatment of $(^{Ar}L)Fe$ with adamantyl azide or mesityl azide led to the formation of the high-spin ($S = 5/2$), three-coordinate imidos $(^{Ar}L)Fe(NAd)$ and $(^{Ar}L)Fe(NMes)$, respectively, as determined by EPR, zero-field ^{57}Fe Mössbauer, magnetometry, and single crystal X-ray diffraction. The high-spin iron imidos are reactive with a variety of substrates: $(^{Ar}L)Fe(NAd)$ reacts with azide yielding a ferrous tetrazido $(^{Ar}L)Fe(\kappa^2\text{-}N_4Ad_2)$, undergoes

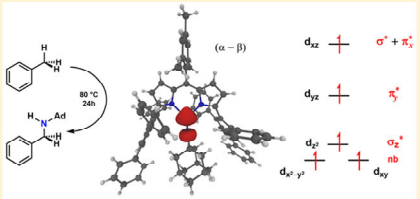

High Spin Imido

J. Am. Chem. Soc. **2017**, *139*, 12043.

Scheme 1

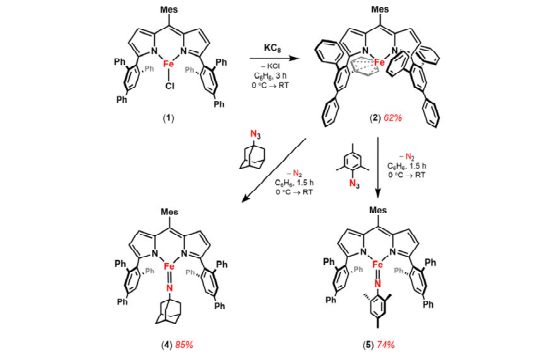

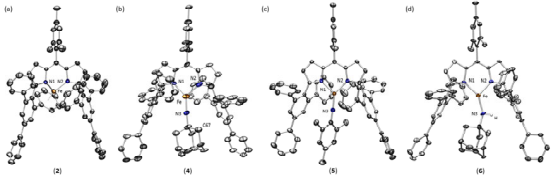

Figure 2. Solid-state structure of (a) (^{Ar}L)Fe (2) and (b) (^{Ar}L)Fe(NAd) (4) at 100 K with 20% probability ellipsoids and (c) (^{Ar}L)Fe(NMes) (5) and (d) (^{Ar}L)Fe(NHAd) (6) at 100 K with 35% probability ellipsoids. H atoms and solvent molecules have been omitted for clarity. Colors: Fe, orange; C, gray; H, white; N, blue.

络合物4：Fe–N键长 1.674 Å，显示典型的双键特征；
络合物5：Fe–N键长 1.708 Å，显示典型的双键特征。

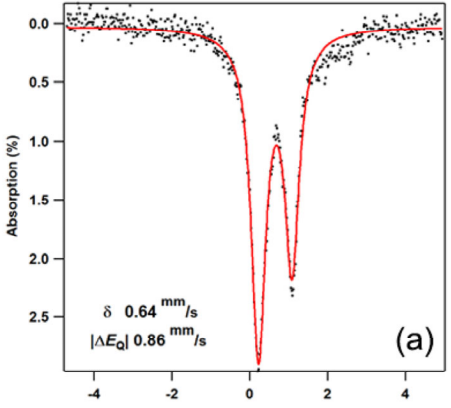

δ = 0.64 mm/s：这个值落在Fe(I)的典型区间（0.5-0.8 mm/s）内。

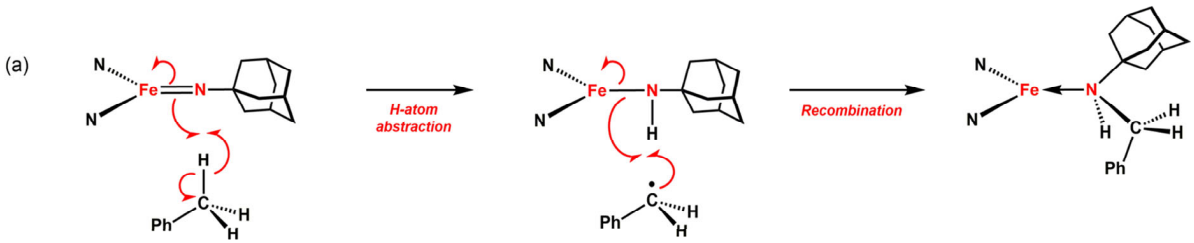

- **动力学同位素效应：**

分子间：k_H/k_D = 15.5(3)

分子内：k_H/k_D = 11(1)

表明C–H键断裂是决速步，支持分步的HAA/自由基重组机制。

协同机理: KIE值小至中等 (通常 2-3)
分步机理: KIE值大(通常 >7)

JACS JOURNAL OF THE AMERICAN CHEMICAL SOCIETY
Article
Cite This: J. Am. Chem. Soc. 2017, 139, 14757-14766
pubs.acs.org/JACS

Direct Comparison of C–H Bond Amination Efficacy through Manipulation of Nitrogen-Valence Centered Redox: Imido versus Iminyl

Matthew J. T. Wilding,[†] Diana A. Iovan,[†] Alexandra T. Wrobel,[†] James T. Lukens,[‡] Samantha N. MacMillan,[‡] Kyle M. Lancaster,[‡] and Theodore A. Betley*[,†]

[†]Department of Chemistry and Chemical Biology, Harvard University, 12 Oxford Street, Cambridge, Massachusetts 02138, United States

[‡]Department of Chemistry and Chemical Biology, Baker Laboratory, Cornell University, Ithaca, New York 14853, United States

Supporting Information

ABSTRACT: Reduction of previously reported iminyl radical (^{Ad}L)FeCl($^{\bullet}$N(C_6H_4-*p*-^{t}Bu)) (**2**) with potassium graphite furnished the corresponding high-spin (S = $^5/_2$) imido (^{Ad}L)Fe(N(C_6H_4-*p*-^{t}Bu)) (**3**) (^{Ad}L = 5-mesityl-1,9-(2,4,6-$Ph_3C_6H_2$)dipyrrin). Oxidation of the three-coordinate imido (^{Ad}L)Fe(NAd) (**5**) with chlorotriphenylmethane afforded (^{Ad}L)FeCl($^{\bullet}$NAd) (**6**) with concomitant expulsion of Ph_3C-(C_6H_5)CPh_2. The respective aryl/alkyl imido/iminyl pairs (**3**, **2**; **5**, **6**) have been characterized by EPR, zero-field ^{57}Fe Mössbauer, magnetometry, single crystal X-ray diffraction,

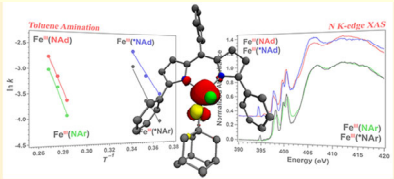

单核金属络合物 (Fe)

Scheme 1. Synthesis of Imido (3, 5) and Iminyl (2, 6) Species

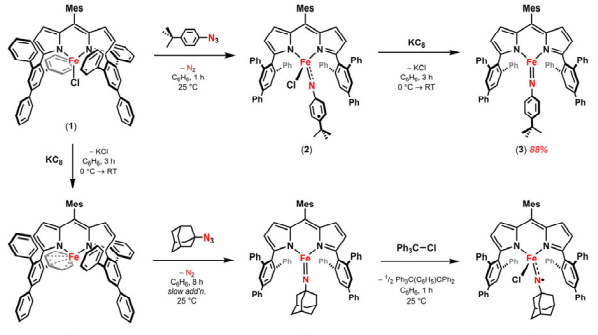

首次合成了烷基亚氨基自由基络合物

Scheme 2. Inter- and Intramolecular Amination Reactions

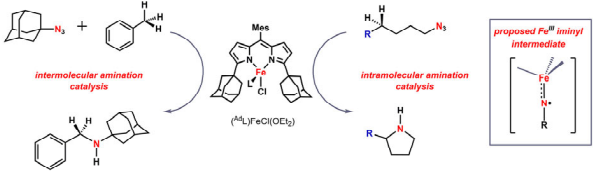

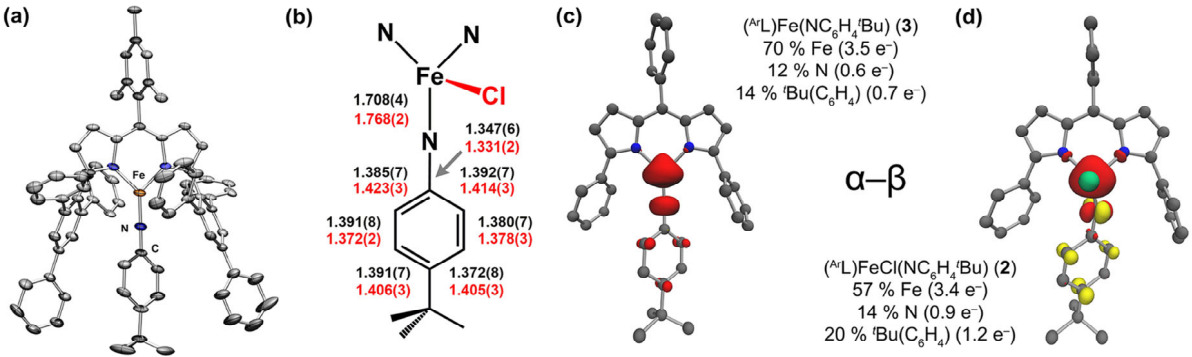

Figure 2. (a) Solid state molecular structure of **3** with thermal ellipsoids at the 35% probability level. Positional disorder, solvent molecules, and H atoms are removed for clarity. Color scheme: Fe, orange; N, blue; C, gray. (b) Selected bond metrics (Å) for iminyl **2** in red and imido **3** in black. Mulliken spin density plots ($\alpha-\beta$) and values calculated for **3** (c) and **2** (d).

Table 3. Rate Constants, Half-Lives, and Activation Energies for Reaction of Iron Complexes with Toluene[a]

complex	T (°C)	k (s^{-1})	$t_{1/2}$ (min)	E_a (kcal/mol)
5	80	0.0264	26	11.5
	90	0.0427	16	
	100	0.0633	11	
3	80	0.0195	36	12.1
	90	0.0343	20	
	100	0.0745	9	
6	22	0.0299	23	7.1
	32	0.0433	16	
	42	0.0722	10	
2	22	0.0166	42	9.2
	32	0.0256	27	
	42	0.0528	13	

[a]Exponential decay of $\Delta(\lambda_{max})$ versus time was fit independently at each temperature.

GDCh Communications Angewandte International Edition Chemie

Radical Reactions

International Edition: DOI: 10.1002/anie.201706594
German Edition: DOI: 10.1002/ange.201706594

C–H Activation from Iron(II)-Nitroxido Complexes

*Claudia Kleinlein, Andrew J. Bendelsmith, Shao-Liang Zheng, and Theodore A. Betley**

Abstract: *The reaction of nitroxyl radicals TEMPO (2,2′,6,6′-tetramethylpiperidinyloxyl) and AZADO (2-azaadamantane-N-oxyl) with an iron(I) synthon affords iron(II)-nitroxido complexes* (^{Ar}L)*Fe*(κ^1*-TEMPO) and* (^{Ar}L)*Fe*(κ^2*-N,O-AZADO)* (^{Ar}L *= 1,9-(2,4,6-*$Ph_3C_6H_2$*)*$_2$*-5-mesityldipyrromethene). Both high-spin iron(II)-nitroxido species are stable in the absence of weak C–H bonds, but decay via N–O bond homolysis to ferrous or ferric iron hydroxides in the presence of 1,4-cyclohexadiene. Whereas* (^{Ar}L)*Fe*(κ^1*-TEMPO) reacts to give a diferrous hydroxide [*(^{Ar}L)*Fe*$]_2(\mu\text{-}OH)_2$*, the reaction of four-coordinate* (^{Ar}L)*Fe*(κ^2*-N,O-AZADO) with hydrogen atom donors yields ferric hydroxide* (^{Ar}L)*Fe(OH)(AZADO). Mechanistic experiments reveal saturation behavior in C–H substrate and are consistent with rate-determining hydrogen atom transfer.*

iron(II)-hydroperoxo and -alkylperoxo model complexes remain elusive to date, due to facile oxidation of the iron(II) site through O–O bond cleavage.[2c,6] Iron(II)-nitroxido complexes can be regarded as isoelectronic, but more stable analogues of peroxo species. We therefore propose that the study of pathways available for N–O bond cleavage in iron(II)-nitroxido complexes can complement the current mechanistic understanding for enzymatic oxidation reactions involving iron(II)-alkylperoxo species (Figure 1b). In 2012, Smith et al. reported an iron(II)-nitroxido species PhB(MesIm)$_3$Fe(κ^1-TEMPO) featuring a tris(carbene)borate ligand (PhB(MesIm)$_3$ = phenyltris(1-mesitylimidazol-2-ylidene)borate).[7] Upon heating, N–O bond homolysis occurred and formation of an iron(III)-oxo complex was proposed.

Herein, we report the synthesis and characterization of

在众多血红素和非血红素酶中，铁(II)-过氧/烷基过氧物种是关键的氧化反应中间体。

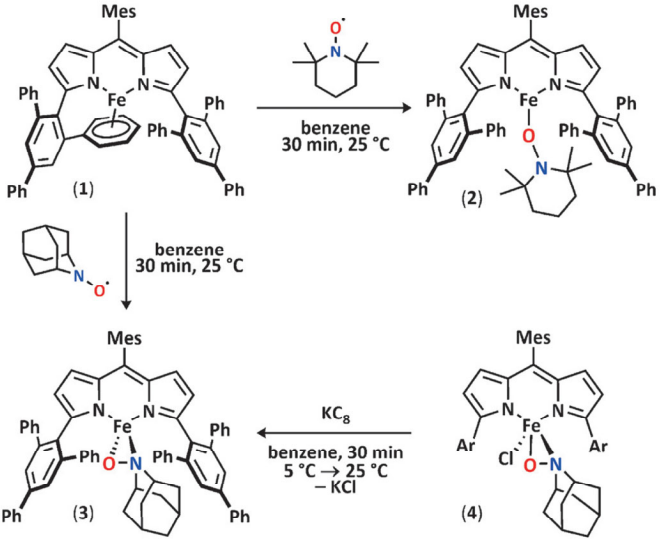

Scheme 1. Synthesis of iron nitroxides.

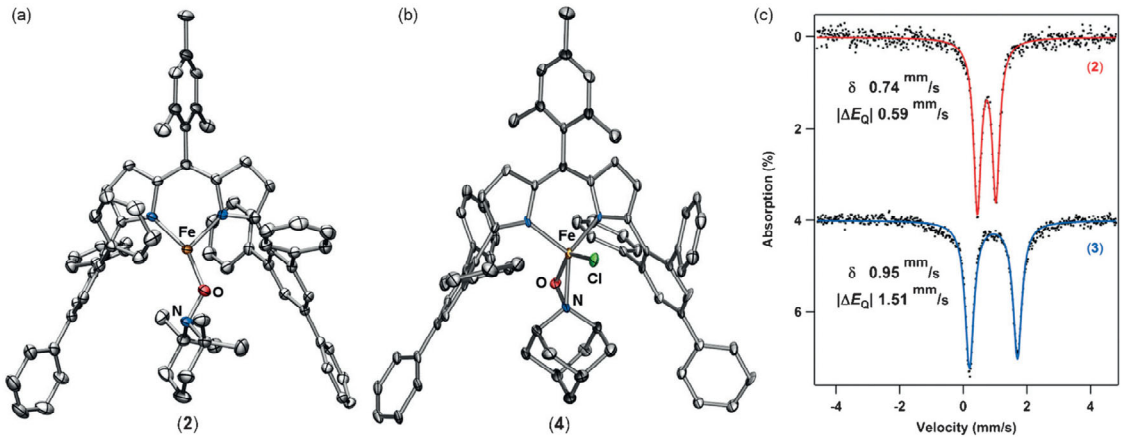

Figure 2. Solid-state structures of a) (^{Ar}L)Fe(κ^1-TEMPO) (**2**) and b) (^{Ar}L)FeCl(κ^2-N,O-AZADO) (**4**) at 100 K with thermal ellipsoids at 50% probability level. Color Scheme: Fe, orange; N, blue; O, red; Cl, green. Hydrogens and solvent molecules are omitted for clarity. c) Zero-field ^{57}Fe Mössbauer spectrum of (^{Ar}L)Fe(κ^1-TEMPO) (**2**) (red, top) and (^{Ar}L)Fe(κ^2-N,O-AZADO) (**3**) (blue, bottom) collected at 90 K.

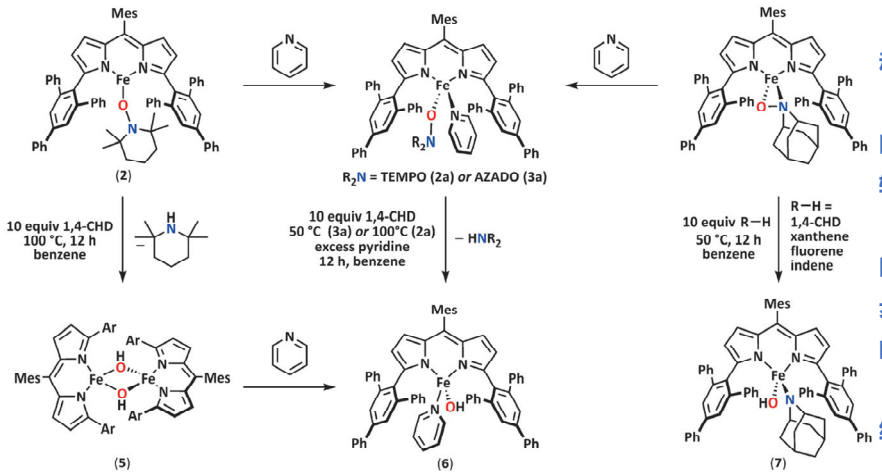

Scheme 2. Formation of iron hydroxides.

动力学同位素效应 (KIE):

（1）当xanthene = 5 equiv时，KIE ≈ 6.1，表明氢原子转移是决速步。

（2）当xanthene = 50 equiv时，KIE降至2.1，表明决速步转变为不涉及C–H键断裂的步骤。

结论：更有可能是协同机理。

C–H Activation

International Edition: DOI: 10.1002/anie.201708519
German Edition: DOI: 10.1002/ange.201708519

Diastereoselective C–H Bond Amination for Disubstituted Pyrrolidines

*Diana A. Iovan, Matthew J. T. Wilding, Yunjung Baek, Elisabeth T. Hennessy, and Theodore A. Betley**

Abstract: *We report herein the improved diastereoselective synthesis of 2,5-disubstituted pyrrolidines from aliphatic azides. Experimental and theoretical studies of the C–H amination reaction mediated by the iron dipyrrinato complex (^{Ad}L)FeCl(OEt$_2$) provided a model for diastereoinduction and allowed for systematic variation of the catalyst to enhance selectivity. Among the iron alkoxide and aryloxide catalysts evaluated, the iron phenoxide complex exhibited superior performance towards the generation of syn 2,5-disubstituted pyrrolidines with high diastereoselectivity.*

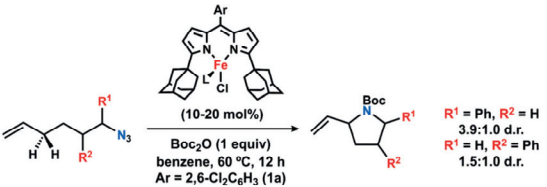

Scheme 1. Diastereoselective iron-catalyzed cyclization.

Table 1: Diastereoselective C–H amination.

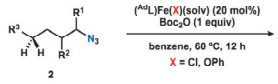

Product	Yield [%][a]	d.r.[b]	Product	Yield [%][a]	d.r.[b]	Product	Yield [%][a]	d.r.[b]
$R^3 = C_2H_1$			$R^3 = C_2H_1$			$R^3 = C_2H_1$		
3a	(72)[c] 77 (72)[d]	3.9:1[c] >20:1[d]	3f	36 (36)[c] 53 (53)[d]	4:1[c] 20:1[d]	3k	30 (30)[c,e] 52 (45)[d]	>20:1[c] >20:1[d]
3b	(63)[c] 75 (67)[d]	3:1[c] >20:1[d]	3g	(47)[c] 55 (49)[d]	4:1[c] >20:1[d]	3l	37 (36)[c] 58 (56)[d]	>20:1[c] >20:1[d]
3c	44 (41)[c] 67 (68)[d]	4:1[c] >20:1[d]	3h	59 (55)[c] 79 (72)[d]	4:1[c] >20:1[d]	3m	38 (31)[c] 58 (51)[d]	>20:1[c] >20:1[d]
3d	(49)[c] 67 (66)[d]	3:1[c] >20:1[d]	3i	64 (48)[c] 74 (67)[d]	4:1[c] >20:1[d]	3n	27 (30)[c] 50 (43)[d]	4:1[c] 11:1[d]
3e	38 (41)[c] 74 (71)[d]	3:1[c] >20:1[d]	3j	45 (38)[c] 69 (64)[d]	>20:1[c] >20:1[d]	3o	22 (16)[c] 20 (23)[d]	3:1[c] 10:1[d]
$R^1 = Ph, R^3 = Ph$			$R^1 = C_2H_3, R^3 = Ph$			$R^1 = H, R^2 = Ph, R^3 = C_2H_3$		
3p	34 (37)[c] 43 (48)[d]	5:1[c] 16:1[d]	3q	N/A	3.5:1[c] 7:1[d]	3r	(66)[c] 71 (72)[d]	1.5:1[c] 2:1[d]

[a] ^{1}H NMR yield (isolated yields in parentheses). [b] *syn*:*anti*. [c] Catalyst **1a**. [d] Catalyst **8**. [e] 10 mol% catalyst.

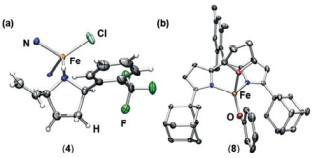

Figure 1. Truncated solid state structure[10] of a) (^{Ad}L)FeCl [2-(*o*-(F$_3$C)C$_6$H$_3$)-5-vinylpyrrolidine] (**4**) and b) (^{Ad}L)Fe(OPh)(THF) (**8**) at 100 K with 50% probability ellipsoids.

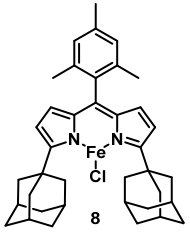

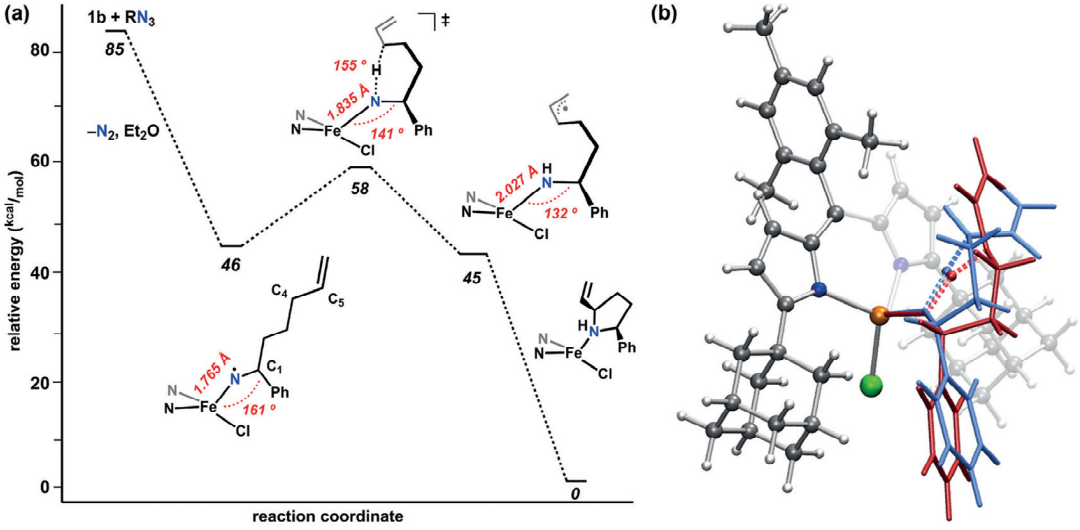

Figure 2. a) Calculated[12] reaction coordinate for cyclization of 1-azido-1-phenyl-hex-5-ene (**2a**) mediated by **1b**. b) Geometry-optimized TS for the HAA step in the pro-*syn* (blue) and pro-*anti* (red) configuration.

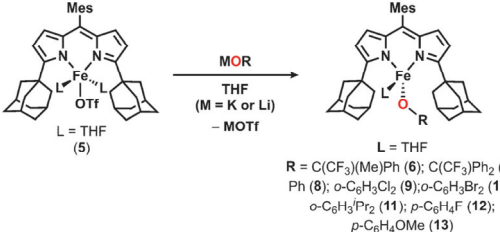

Scheme 2. Synthesis of catalyst variants.

Table 2: Catalyst screening as a function of ancillary ligand.

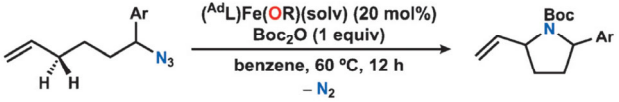

R	Complex	Yield [%]	d.r.[c]
C(CF$_3$)(Me)Ph	**6**	54[a]	13:1
C(CF$_3$)Ph$_2$	**7**	26[a]	6:1
Ph	**8**	67[a]	> 20:1
o-C$_6$H$_3$Cl$_2$	**9**	42[b]	16:1
o-C$_6$H$_3$Br$_2$	**10**	42[b]	> 20:1
o-C$_6$H$_3$*i*Pr$_2$	**11**	49[b]	> 20:1
p-C$_6$H$_4$F	**12**	66[a]	> 20:1
p-C$_6$H$_4$OMe	**13**	82[a]	> 20:1

Catalysts **6**–**8**: reaction with 1-azido-1-(4-chlorophenyl)-hex-5-ene (**2b**); **9**–**13**: reaction with 1-azido-1-phenyl-hex-5-ene (**2a**); [a] Isolated yields. [b] ^{1}H NMR yields. [c] *syn*:*anti*.

JACS
JOURNAL OF THE AMERICAN CHEMICAL SOCIETY
pubs.acs.org/JACS
Article

O-Heterocycle Synthesis via Intramolecular C−H Alkoxylation Catalyzed by Iron Acetylacetonate

Yuyang Dong, Alexandra T. Wrobel, Gerard J. Porter, Jessica J. Kim, Jake Z. Essman, Shao-Liang Zheng, and Theodore A. Betley*

Cite This: J. Am. Chem. Soc. 2021, 143, 7480−7489
Read Online
ACCESS | Metrics & More | Article Recommendations | Supporting Information

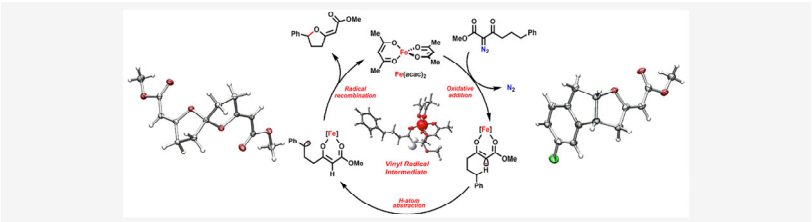

J. Am. Chem. Soc. **2021**, *143*, 7480

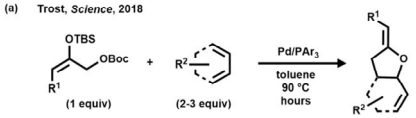

berkelic acid
anticancer activity

(-)-dihydro aflatoxin D_2
antimicrobial carcinogenic toxin

anhydroerythromycin A
antibiotics

(a) *Canvassing substrate C-H bond strength accessiblity*

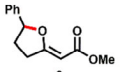

2

a. 30 mol%, 25 °C, 3 h, 58 %
b. 10 mol%, 60 °C, 20 min, 74 %
61 %

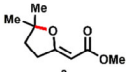

3

5 mol%, 25 °C, 3 h, 86 %
70 %

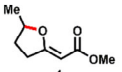

4

a. 30 mol%, 25 °C, 12 h, 88 %
b. 10 mol%, 60 °C, 20 min, 83 %
63 %

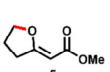

5

30 mol%, 100 °C, 20 min, 49 %
26 % (11:89 Z:E)

(b) *Tracking stepwise reaction through isotope labeling*

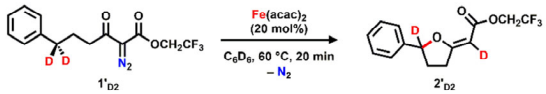

1'$_{D2}$ 2'$_{D2}$

(c) *Radical clock ring opening*

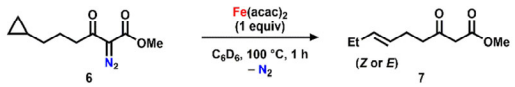

6 7

(d) *Shunt reaction with sacrificial H-atom donor*

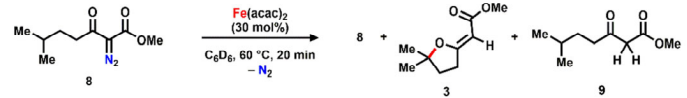

8 3 9

no CHD	0 %	>99 %	<1%
10 equiv CHD	59%	18 %	23 %

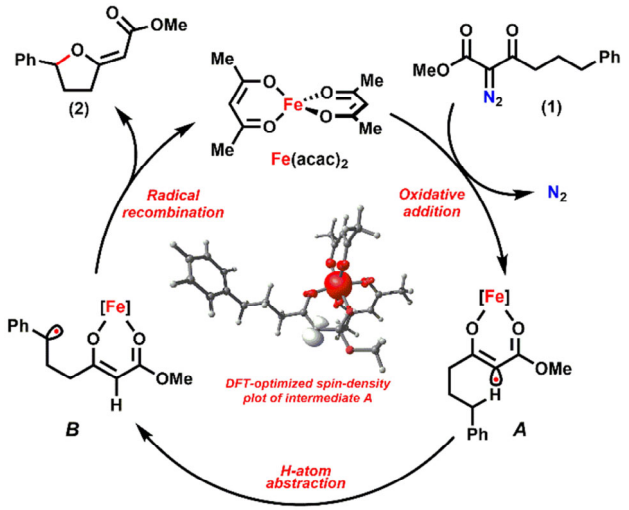

Figure 4. Proposed catalytic mechanism for the synthesis of substituted tetrahydrofurans.

(a) *Chemoselectivity of keto- vs. ester-substituent:*

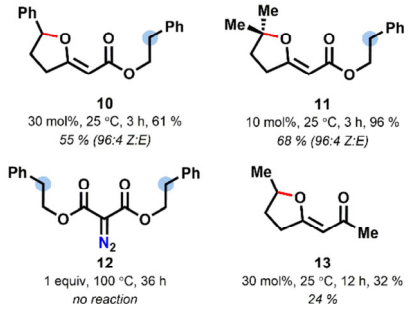

10
30 mol%, 25 °C, 3 h, 61 %
55 % (96:4 Z:E)

11
10 mol%, 25 °C, 3 h, 96 %
68 % (96:4 Z:E)

12
1 equiv, 100 °C, 36 h
no reaction

13
30 mol%, 25 °C, 12 h, 32 %
24 %

(b) *Selectivity between 5- vs. 6-membered ring formation:*

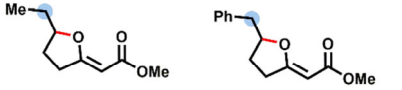

14
a. 30 mol%, 25 °C, 12 h, 77 %
b. 10 mol%, 60 °C, 20 min, 94 %
69 % (94:6 Z:E)

15
a. 30 mol%, 25 °C, 12 h, 63 %
b. 10 mol%, 60 °C, 20 min, 66 %
52 %

(a) *Preparation of spiro-bi- and tricyclic systems:*

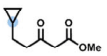

31
1 equiv. 100 °C, 36 h
no reaction

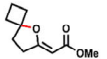

32
10 mol%. 25 °C. 3 h. 86 %
57 % (94:6 Z:E)

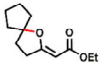

33
10 mol%. 25 °C. 3 h. 83 %
76 % (97:3 Z:E)

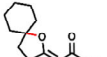

34
10 mol%. 25 °C. 1 h. 74 %
64 % (96:4 Z:E)

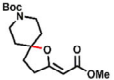

35
10 mol%. 25 °C. 3 h. 71 %
51 %

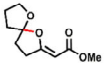

36
15 mol%. 25 °C. 3 h. 77 %
72 %

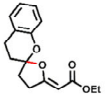

37
10 mol%, 25 °C, 3 h, 94 %
64 % (98:2 Z:E)

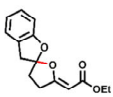

38
20 mol%, 25 °C, 3 h, 58 %
47 %

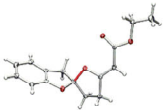

(38)

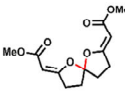

39
30 mol%, 60 °C, 40 min, 48 %
43 %

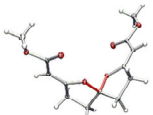

(39)
Double activation of the methylene group

(b) *Regioselective synthesis of fused-bi- and tricyclic motifs (syn:anti > 99:1) :*

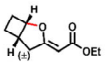

40
syn:anti > 99:1
20 mol%, 25 °C, 3 h, > 99 %
78 %

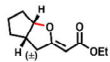

41
syn:anti > 99:1
15 mol%, 25 °C, 3 h, 81 %
73 %

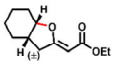

42
syn:anti > 99:1
15 mol%, 25 °C, 3 h, 93 %
69 %

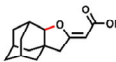

43
20 mol%, 25 °C, 3 h, 80 %
68 % (93:7 Z:E)

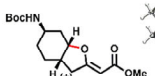

44
syn:anti > 99:1
20 mol%, 25 °C, 3 h, 48 %
43 %

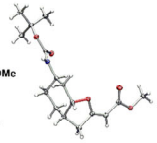

(44)

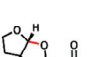

45
syn:anti > 99:1
15 mol%, 25 °C, 3 h, 80 %
73 % (65:15 Z:E)

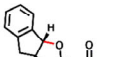

46
syn:anti > 99:1
a. 10 mol%, 25 °C, 3 h, 73 %
b. 10 mol%, 60 °C, 20 min, 75 %
70 %

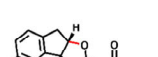

47
syn:anti > 99:1
50 mol%, 100 °C, 20 min, 32 %
25 %

(47)

JACS
JOURNAL OF THE AMERICAN CHEMICAL SOCIETY
pubs.acs.org/JACS Article

An Open-Shell Fe^{IV} Nitrido

Jeewhan Oh, Shao-Liang Zheng, Kurtis M. Carsch, Trevor P. Latendresse, Claire E. Casaday, Brandon M. Campbell, and Theodore A. Betley*

Cite This: *J. Am. Chem. Soc.* 2025, 147, 3174–3184 Read Online

ACCESS | Metrics & More | Article Recommendations | Supporting Information

ABSTRACT: We report the photogeneration and characterization of an open-shell, terminal iron nitrido (^{Em}L)Fe(N) using a sterically encumbered dipyrrin ligand environment. The Fe−N distance in the solid-state, zero-field ^{57}Fe Mössbauer spectrum, and computational analysis are consistent with a triplet electronic ground state of the iron nitrido. Notably, the attenuation of Fe−N multiple bond character through occupying π^*_{Fe-N} enables (i) primary C(sp^3)−H amination, (ii) H_2 cleavage, (iii) aromatic C−C cleavage, and (iv) photocatalytic *N*-atom transfer reactivity. These modes of reactivity have not previously been observed in low-spin Fe(N) analogues.

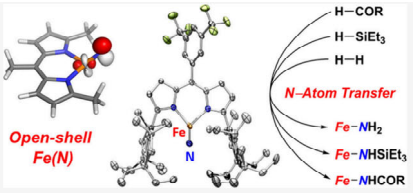

Scheme 1. Metalation of $(^{Em}L)H$ to Synthesize $(^{Em}L)FeCl$ (1), the Preparation of $(^{Em}L)Fe(N_3)$ (2), and the Isolated $C(sp^3)$–H Amination Product (3) via $(^{Em}L)Fe(N)$ (4)

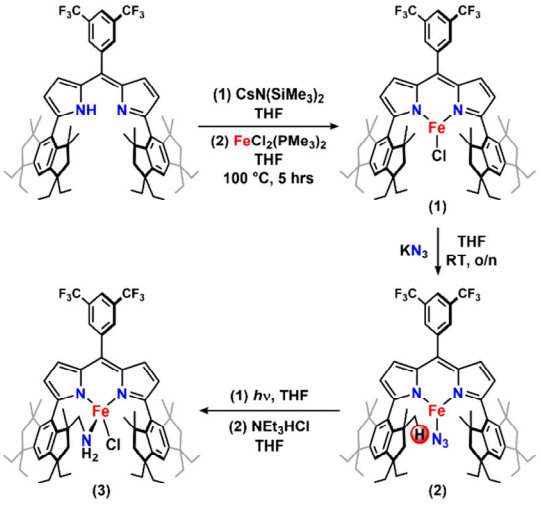

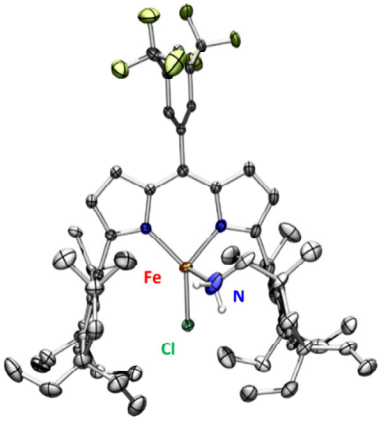

Figure 2. Solid-state structure of $(^{Em}L–NH_2)FeCl$ (3) at 100 K with thermal ellipsoids at the 30% probability level (hydrogen atoms except for those located on the amine fragment and solvent molecules are omitted for clarity; Fe, orange; C, gray; N, blue; F, yellow-green; Cl, green).

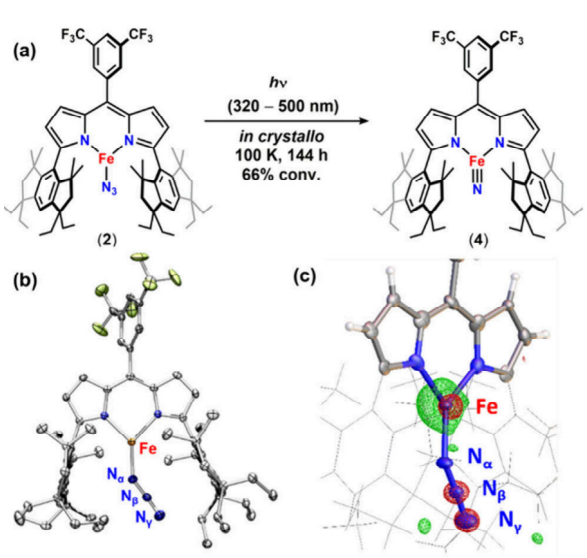

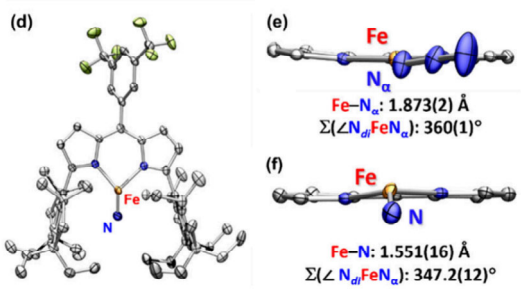

Figure 3. (a) Solid-state conversion of **2** (b) to **4** (d) in crystalline lattice at 100 K with thermal ellipsoids at the 30% probability level (hydrogen atoms and solvent are omitted for clarity; Fe, orange; C, gray; N, blue; F, yellow-green). (c) Electron density difference map[43] (1.7 $e^{-}/Å^{3}$) after the photolysis of **2** for 144 h to generate **4** with rotation of ethyl group from the ligand hydrindacene (green and red colors represent positive and negative electron density, respectively); the core iron environment showing iron pyramidilization prior to photolysis ($\Sigma(\angle N_{dipyrrin}FeN_{\alpha})$: 360(1)°) (e) and following photolysis ($\Sigma(\angle N_{dipyrrin}FeN_{\alpha})$: 347.2(12)°) (f).

Fe–N 键长：1.551(16) Å，比已知低自旋 Fe(IV) 氮宾（1.49–1.53 Å）略长。

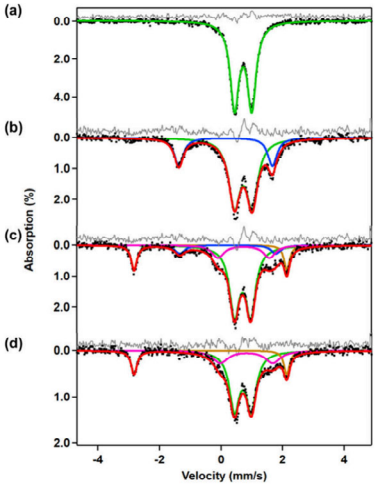

Figure 4. (a) A zero-field ^{57}Fe Mössbauer spectrum of **2** measured at 90 K, (b) **4**−^{57}Fe generated by the irradiation of frozen C_6D_6 solution of **2**−^{57}Fe at 77 K, (c) and (d) after warming **4**−^{57}Fe up to 200 and 240 K for 48 h, respectively; green, $(^{Em}L)^{57}Fe(N_3)$; blue, $(^{Em}L)^{57}Fe(N)$; yellow, thermally excited $(^{Em}L)^{5/}Fe(N)$; pink, $(^{Em}L{-}NH)Fe$; red, fit; and gray, residual.

(b) 69% 2, 31% 4

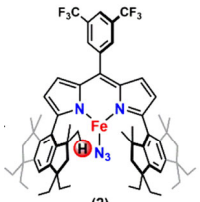

(2)
green

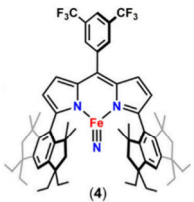

(4)
blue

$\delta = 0.15$ mm/s, $|\Delta E_Q| = 3.03$ mm/s

(d) 61% 2, 13.5% 3

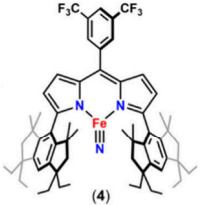

(4)
Yellow-excited

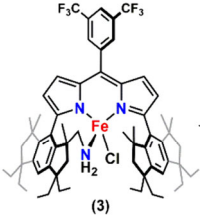

(3)
Pink

Scheme 2. Reaction of 4 with CO, PMe_3, 1,4-CHD, Aldehyde, H_2, $HSiEt_3$, and $CoCp_2$

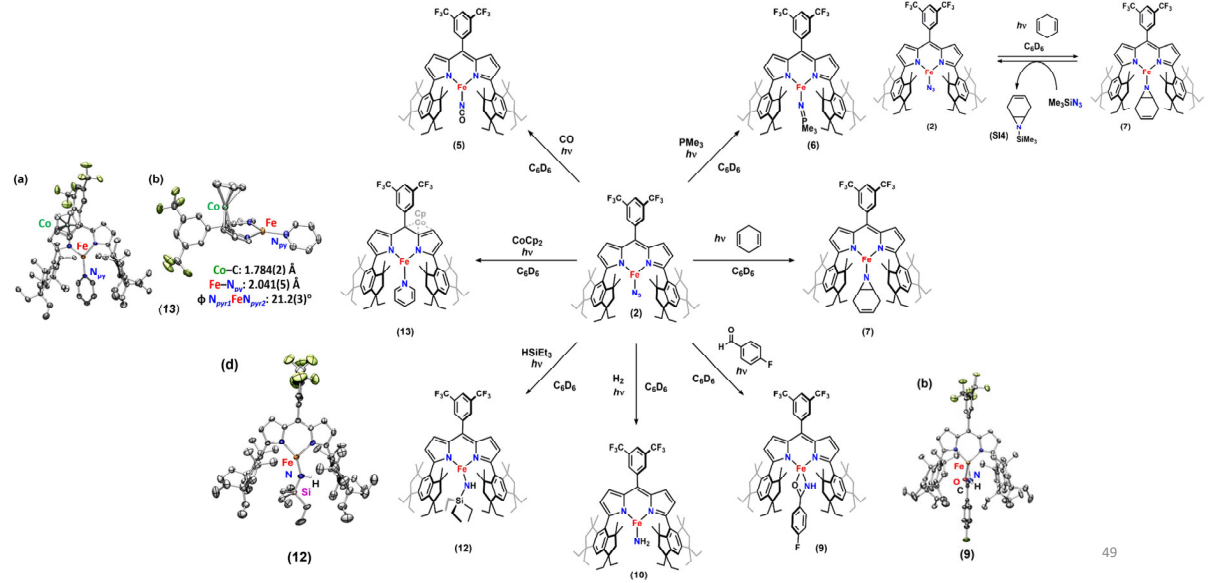

JACS
JOURNAL OF THE AMERICAN CHEMICAL SOCIETY
Communication
pubs.acs.org/JACS

Co(III) Imidos Exhibiting Spin Crossover and C−H Bond Activation

Evan R. King, Graham T. Sazama, and Theodore A. Betley*

Department of Chemistry and Chemical Biology, Harvard University, 12 Oxford Street, Cambridge, Massachusetts 02138, United States

Supporting Information

Scheme 1. Reactions of Co^{I} Synthon 2

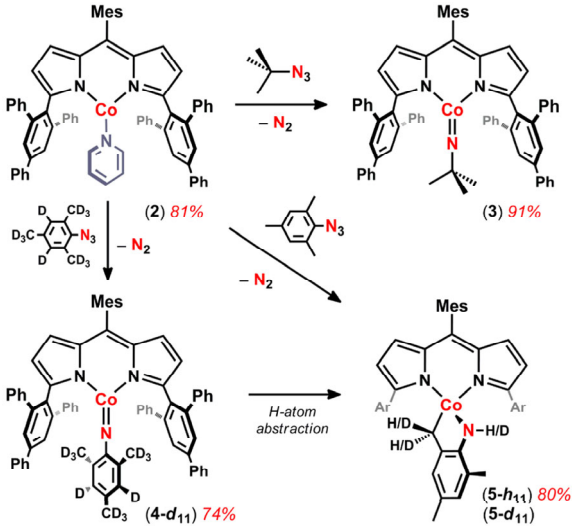

不具备分子间C–H键活化能力。

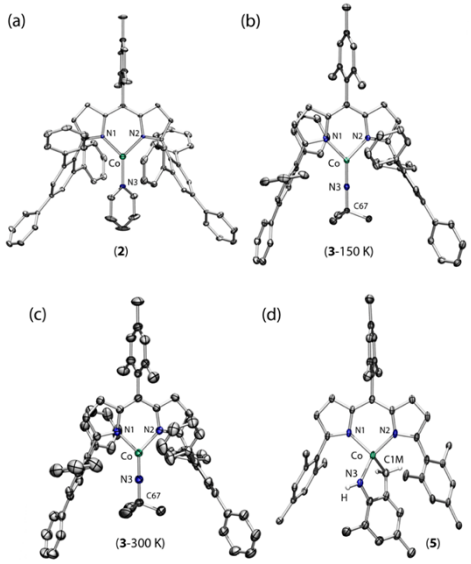

JACS JOURNAL OF THE AMERICAN CHEMICAL SOCIETY
Article
Cite This: J. Am. Chem. Soc. 2019, 141, 7797−7806
pubs.acs.org/JACS

Catalytic C−H Amination Mediated by Dipyrrin Cobalt Imidos

Yunjung Baek and Theodore A. Betley*

Department of Chemistry and Chemical Biology, Harvard University, 12 Oxford Street, Cambridge, Massachusetts 02138, United States

Supporting Information

ABSTRACT: Reduction of (^{Ar}L)Co^{II}Br (^{Ar}L = 5-mesityl-1,9-(2,4,6-$Ph_3C_6H_2$)dipyrrin) with potassium graphite afforded the novel Co^{I} synthon (^{Ar}L)Co^{I}. Treatment of (^{Ar}L)Co^{I} with a stoichiometric amount of various alkyl azides (N_3R) furnished three-coordinate Co^{III} alkyl imidos (^{Ar}L)Co(NR), as confirmed by single-crystal X-ray diffraction (R: CMe_3Bu, $CMe_3(CH_2)_3CHMe_2$). The exclusive formation of four-coordinate cobalt tetrazido complexes (^{Ar}L)Co(κ^2-N_4R_2) was observed upon addition of excess azide, inhibiting any subsequent C−H amination. However, when a weak C−H bond is appended to the imido moiety, as in the case of (4-azido-4-methylpentyl)benzene, intramolecular C−H amination kinetically outcompetes formation of the corresponding tetrazene species to generate 2,2-dimethyl-5-phenylpyrrolidine in a catalytic fashion without requiring product sequestration. The imido

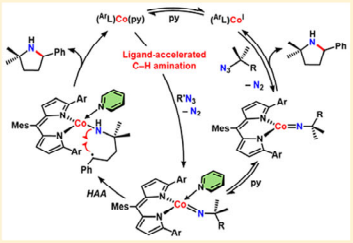

Scheme 1. Synthesis of 2

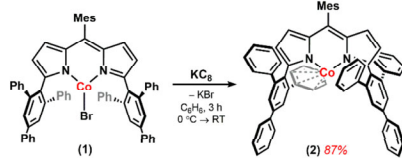

Scheme 2. Reactivity between 2 and Various Linear Alkyl Azides

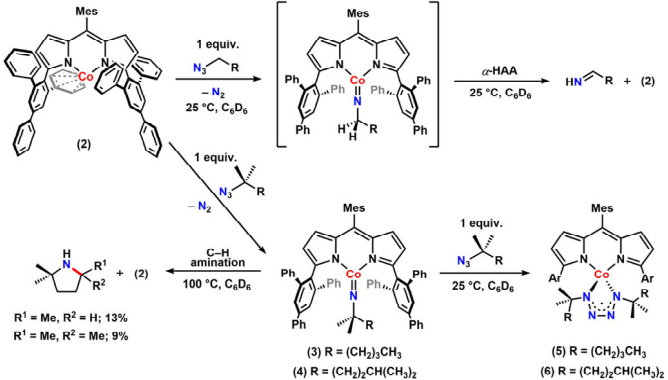

Scheme 3. Intramolecular C−H Amination of Benzylic C−H Bonds

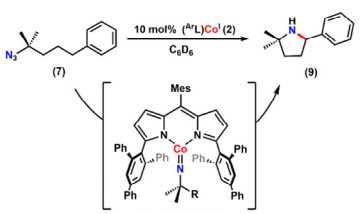

Table 1. Effect of Pyridine Concentration on C−H Amination Reactivity[a]

entry	[py-d_5] (mM)	rate (mM/min)	yield (%)[b]
1	0	N/A[c]	<10
2	4.3	0.52(3)	21
3	8.5	0.70(5)	22
4	26	0.813(5)	35
5	89	1.12(2)	89
6	174	1.45(4)	91
7	300	1.63(4)	93
8	430	1.77(3)	93

[a]Reactions were conducted with pyridine-d_5 to manipulate kinetic experiments with ^{1}H NMR spectroscopy. In all cases, [2] = 4.25 mM and [7] = 85.0 mM in benzene-d_6 at 25 °C. [b]^{1}H NMR yields using 1,3,5-trimethoxybenzene as an internal standard. [c]Initial rate is not available due to a slower formation of **9** at 25 °C.

Scheme 4. Proposed Catalytic Cycle

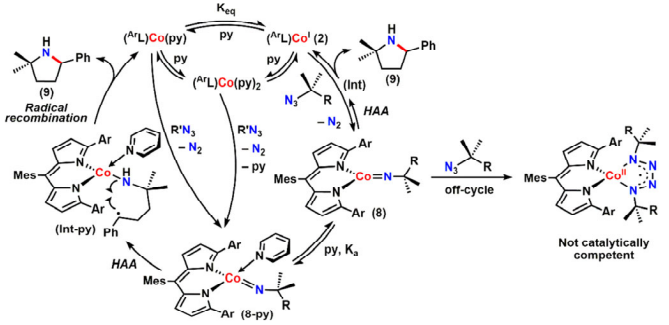

（1）反应速率对亚胺基浓度为一级，对底物叠氮浓度为零级，证明反应是单分子的分子内过程。

（2）KIE ≈ 7.6，证实C–H键断裂是决速步。8是resting state。

（3）Py的加入抑制四氮唑的形成，同时加快反应速率。

（4）与铁相比，无需对产物进行Boc保护来再生催化剂。

JACS JOURNAL OF THE AMERICAN CHEMICAL SOCIETY
Cite This: J. Am. Chem. Soc. 2019, 141, 16944−16953
Article
pubs.acs.org/JACS

Direct Manipulation of Metal Imido Geometry: Key Principles to Enhance C−H Amination Efficacy

Yunjung Back, Elisabeth T. Hennessy, and Theodore A. Betley*

Department of Chemistry and Chemical Biology, Harvard University, 12 Oxford Street, Cambridge, Massachusetts 02138, United States

Supporting Information

ABSTRACT: We report the catalytic C−H amination mediated by an isolable Co^{III} imido complex (^{Tr}L)Co(NR) supported by a sterically demanding dipyrromethene ligand (^{Tr}L = 5-mesityl-1,9-(trityl)dipyrrin). Metalation of (^{Tr}L)Li with $CoCl_2$ in THF afforded a high-spin (S = 3/2) three-coordinate complex (^{Tr}L)CoCl. Chemical reduction of (^{Tr}L)CoCl with potassium graphite yielded the high-spin (S = 1) Co^{I} synthon (^{Tr}L)Co which is stabilized through an intramolecular η^6-arene interaction. Treatment of (^{Tr}L)Co with a stoichiometric amount of 1-azidoadamantane (AdN_3) furnished a three-coordinate, diamagnetic Co^{III} imide (^{Tr}L)-

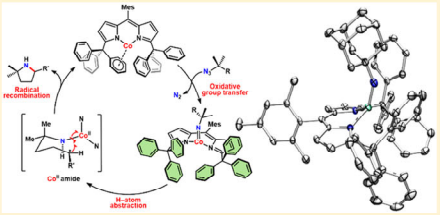

J. Am. Chem. Soc. **2019**, *141*, 16944

Scheme 1. Ligand and Metal Complex Syntheses

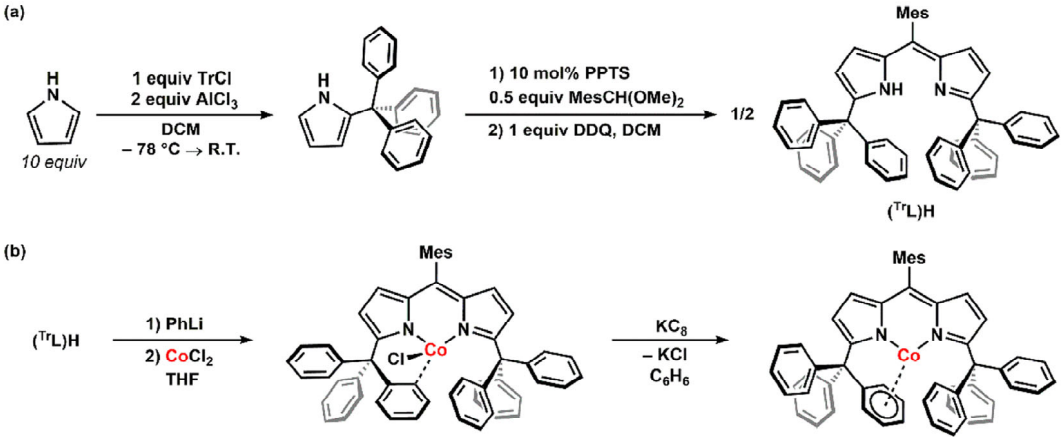

Scheme 2. Reactivity Assessment of 2

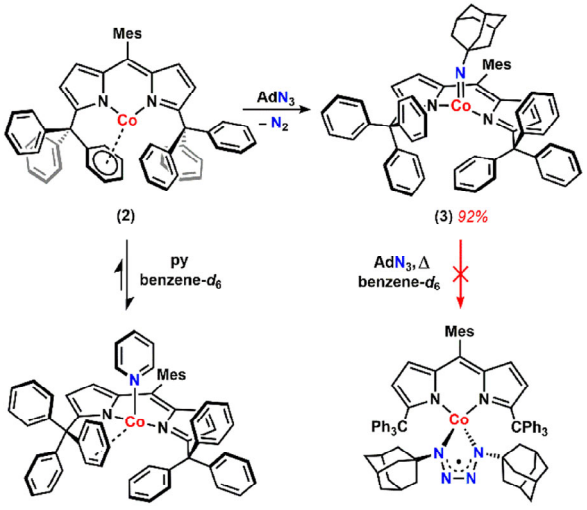

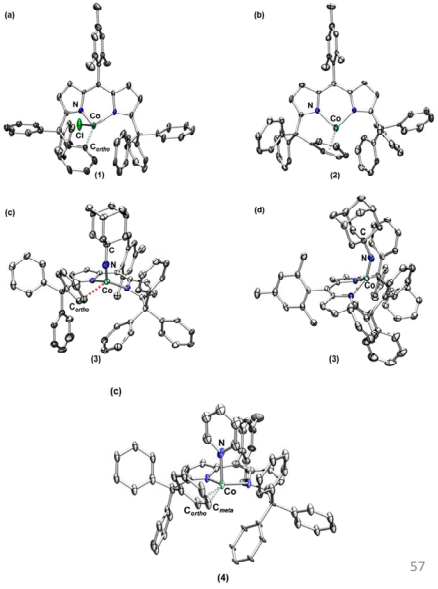

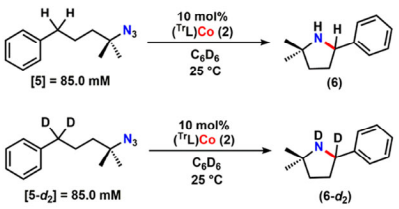

Figure 7. Kinetic isotope effect experiments with 10 mol % of **2** at 25 °C in benzene-d_6.

Scheme 3. Proposed Catalytic Cycle

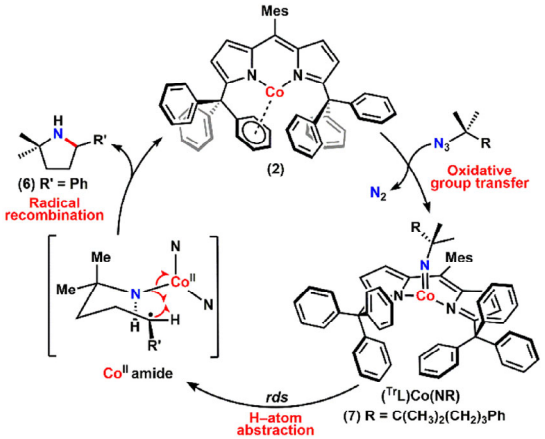

•动力学同位素效应：k_H/k_D = 38.4，表明C–H键断裂是决速步；

•反应级数分析：对底物为零级，对亚胺基为一级，说明反应为单分子HAA过程；

Table 1. Catalytic C–H Amination Using 2 and Alkyl Azides[a]

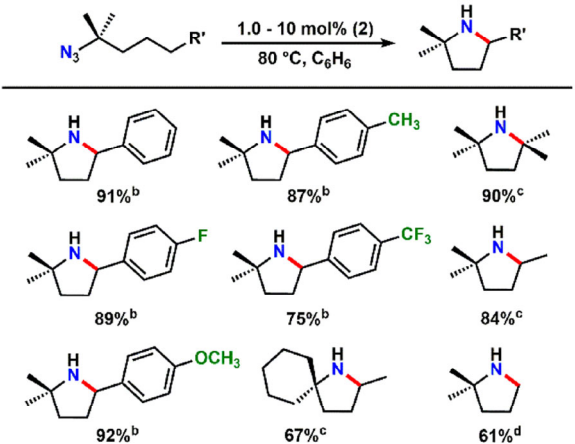

[a]Isolated yields from reactions conducted with 85.0 mM of azide substrate. [b]1 mol % of **2**. [c]5 mol % of **2**. [d]10 mol % of **2**.

JACS
JOURNAL OF THE AMERICAN CHEMICAL SOCIETY
pubs.acs.org/JACS
Article

C–H Amination Mediated by Cobalt Organoazide Adducts and the Corresponding Cobalt Nitrenoid Intermediates

Yunjung Baek, Anuvab Das, Shao-Liang Zheng, Joseph H. Reibenspies, David C. Powers, and Theodore A. Betley*

Cite This: *J. Am. Chem. Soc.* 2020, 142, 11232–11243
Read Online
ACCESS | Metrics & More | Article Recommendations | Supporting Information

ABSTRACT: Treatment of (^{Ar}L)CoBr (^{Ar}L = 5-mesityl-1,9-(2,4,6-$Ph_3C_6H_2$)dipyrrin) with a stoichiometric amount of 1-azido-4-(*tert*-butyl)benzene $N_3(C_6H_4$-*p*-^{t}Bu) furnished the corresponding four-coordinate organoazide-bound complex (^{Ar}L)CoBr($N_3(C_6H_4$-*p*-^{t}Bu)). Spectroscopic and structural characterization of the complex indicated redox innocent ligation of the organoazide. Slow expulsion of dinitrogen (N_2) was observed at room temperature to afford a ligand functionalized product via a [3 + 2] annulation, which can be mediated by a high-valent nitrene intermediate such as a Co^{III} iminyl (^{Ar}L)CoBr($^{\bullet}N(C_6H_4$-*p*-^{t}Bu)) or Co^{IV} imido (^{Ar}L)CoBr($N(C_6H_4$-*p*-^{t}Bu)) complex. The presence of the proposed intermediate and its viability as a nitrene group transfer

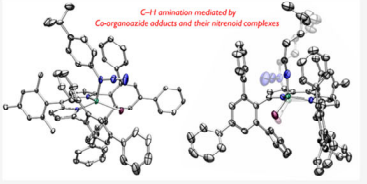

J. Am. Chem. Soc. **2020**, *142*, 11232

Scheme 1. Synthesis of 3

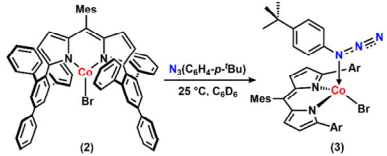

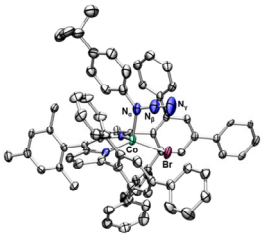

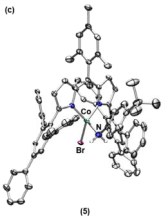

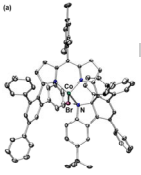

Scheme 2. Intra- and Intermolecular Nitrene Group Transfer Reactivity of 3

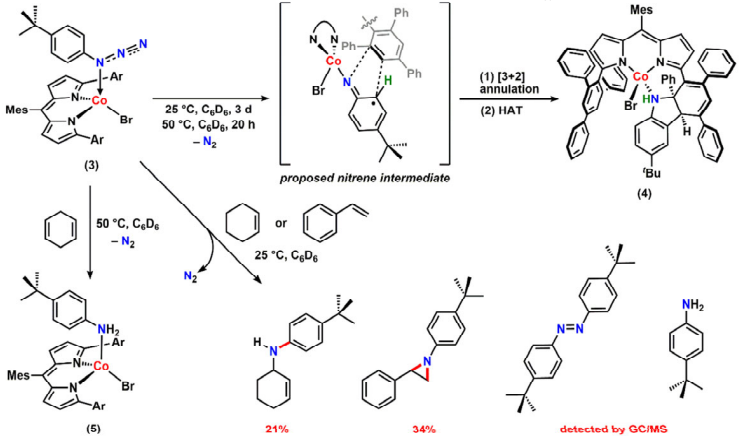

Scheme 3. Synthesis and Reactivity of Dipyrrinato Co^{II} Alkyl Azide Adduct Complexes

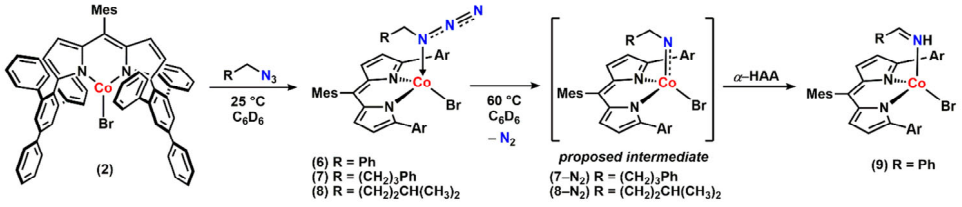

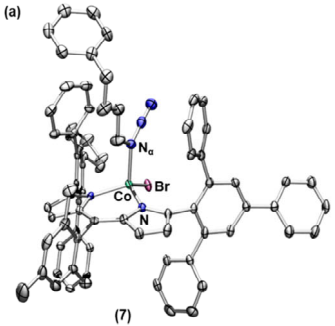

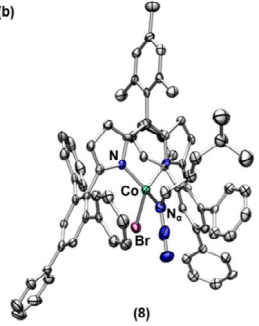

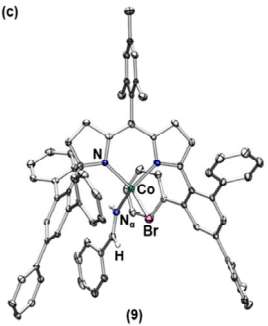

Scheme 4. Synthesis of 10, 11, and 12

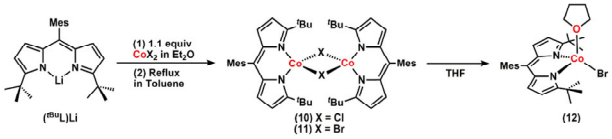

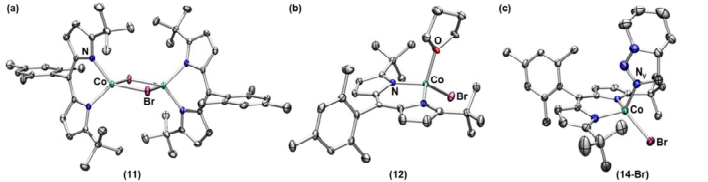

Figure 7. (a) Solid-state structures for (a) **11**, (b) **12**, and (c) **14-Br** at 100 K with thermal ellipsoids at the 50% probability level (hydrogen atoms and solvent molecules are omitted for clarity; Co, aquamarine; C, gray; N, blue; O, red; and Br, maroon).

Scheme 5. 1,3-Dipolar Cycloaddition Reactivity

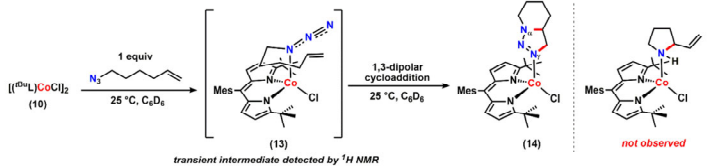

Scheme 6. Intramolecular C–H Amination or Activation

(a) C–H amination in the presence of weak C–H bonds at C_4 position

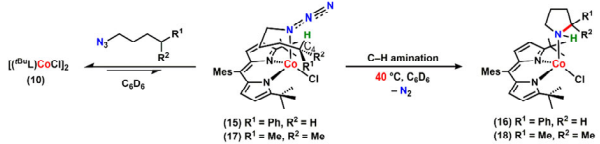

(b) α–H–atom abstraction in the absence of weak C–H bonds at C_4 position

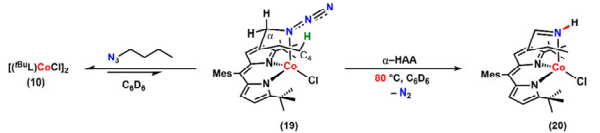

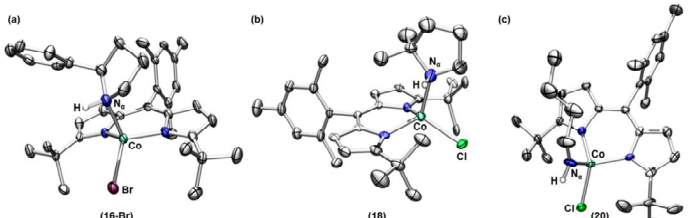

Scheme 8. Proposed Pathways for Intramolecular C–H Amination or Activation

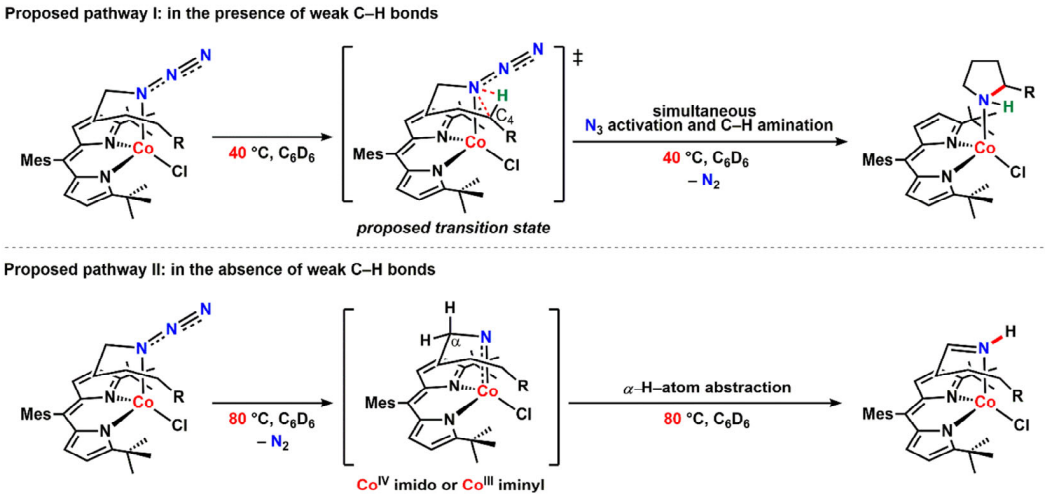

叠氮加合物本身可以直接作为C-H胺化的试剂，而不一定需要先解离N_2形成一个离散的高价钴-氮宾中间体。

INORGANIC CHEMISTRY

Synthesis of a copper-supported triplet nitrene complex pertinent to copper-catalyzed amination

Kurtis M. Carsch[1], Ida M. DiMucci[2], Diana A. Iovan[1], Alex Li[1], Shao-Liang Zheng[1], Charles J. Titus[3], Sang Jun Lee[4], Kent D. Irwin[3,5], Dennis Nordlund[4], Kyle M. Lancaster[2]*, Theodore A. Betley[1]*

Terminal copper-nitrenoid complexes have inspired interest in their fundamental bonding structures as well as their putative intermediacy in catalytic nitrene-transfer reactions. Here, we report that aryl azides react with a copper(I) dinitrogen complex bearing a sterically encumbered dipyrrin ligand to produce terminal copper nitrene complexes with near-linear, short copper–nitrenoid bonds [1.745(2) to 1.759(2) angstroms]. X-ray absorption spectroscopy and quantum chemistry calculations reveal a predominantly triplet nitrene adduct bound to copper(I), as opposed to copper(II) or copper(III) assignments, indicating the absence of a copper–nitrogen multiple-bond character. Employing electron-deficient aryl azides renders the copper nitrene species competent for alkane amination and alkene aziridination, lending further credence to the intermediacy of this species in proposed nitrene-transfer mechanisms.

Science **2019**, *365*, 1138.

侧基为 EMind基团，具有庞大的四面体结构和多个甲基，能有效屏蔽铜中心，防止二聚或氮宾解离。

A

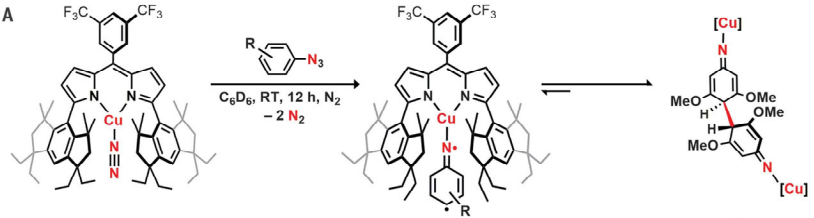

(1)

(2') R = 3,5-$(OMe)_2C_6H_3$
(3) R = 4-$(O^tBu)C_6H_4$
(4) R = 4-$(^tBu)C_6H_4$

(2)

B

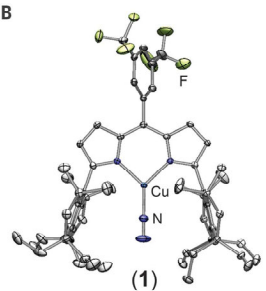

(1)

C

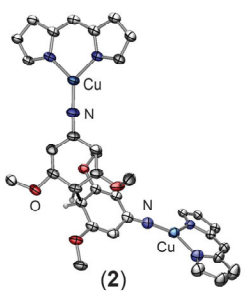

(2)

D

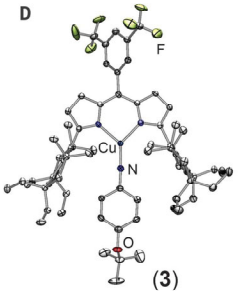

(3)

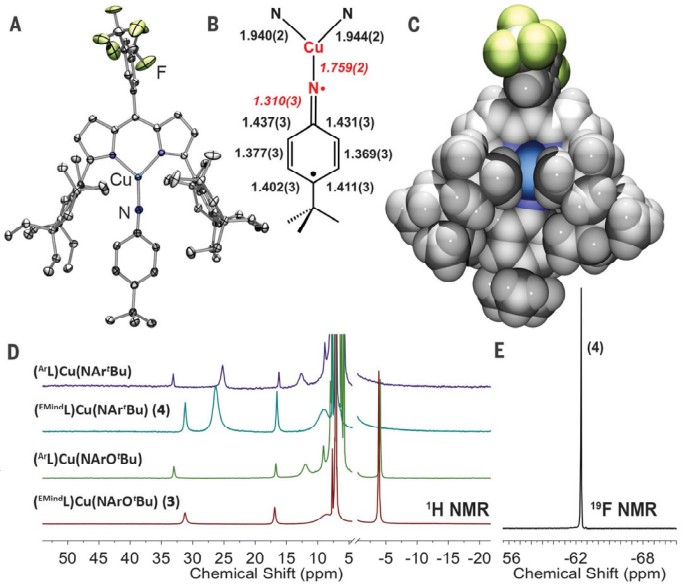
A
F
Cu
N
B
N
N
1.940(2)
Cu
1.944(2)
1.759(2)
N•
1.310(3)
1.437(3)
1.431(3)
1.377(3)
1.369(3)
1.402(3)
1.411(3)
C
D
(ArL)Cu(NArtBu)
(FMIndL)Cu(NArtBu) (4)
(ArL)Cu(NArOtBu)
(EMIndL)Cu(NArOtBu) (3)
1H NMR
50 45 40 35 30 25 20 15 10 5 -5 -10 -15 -20
Chemical Shift (ppm)
E
(4)
19F NMR
56 -62 -68
Chemical Shift (ppm)

顺磁性，三线态

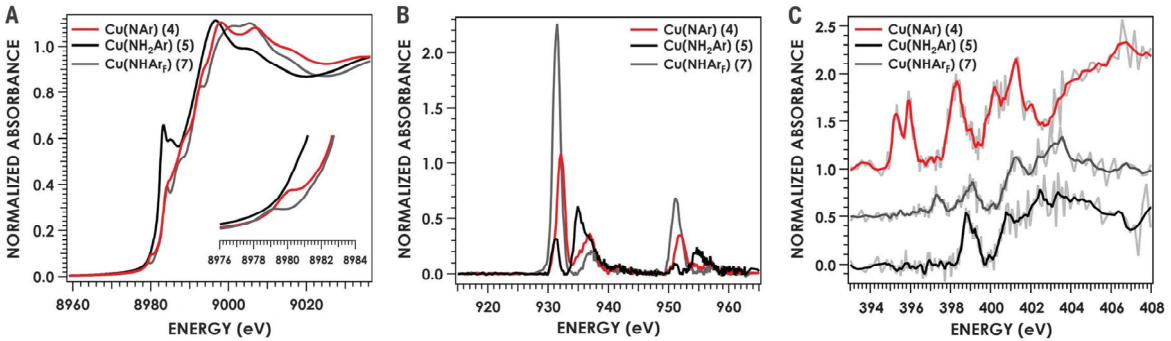

Fig. 4. XAS. (**A**) Cu K-edge, (**B**) Cu $L_{2,3}$-edge, and (**C**) N K-edge absorption spectra of (^{EMind}L)Cu[N($C_6H_4{}^tBu$)] (**4**, red), (^{EMind}L)Cu[H_2N($C_6H_4{}^tBu$)] (**5**, black), (^{EMind}L)Cu{HN[3,5-$(CF_3)_2C_6H_3$]} (**7**, gray). Light-gray lines in (C) represent experimental data, with colored lines representing smoothed data.

- Cu(I) 参考物 5：吸收边在 8992.1 eV
- Cu(II) 参考物 7：吸收边在 8995.0 eV
- 目标氮宾物 4：吸收边在 8995.7 eV

Cu等重金属元素，K-edge能量受配体性质影响很大，不能单独作为氧化态的绝对判据。

信号非常强。其强度直接正比于未占据的3d轨道的空穴数量。

三线态氮宾

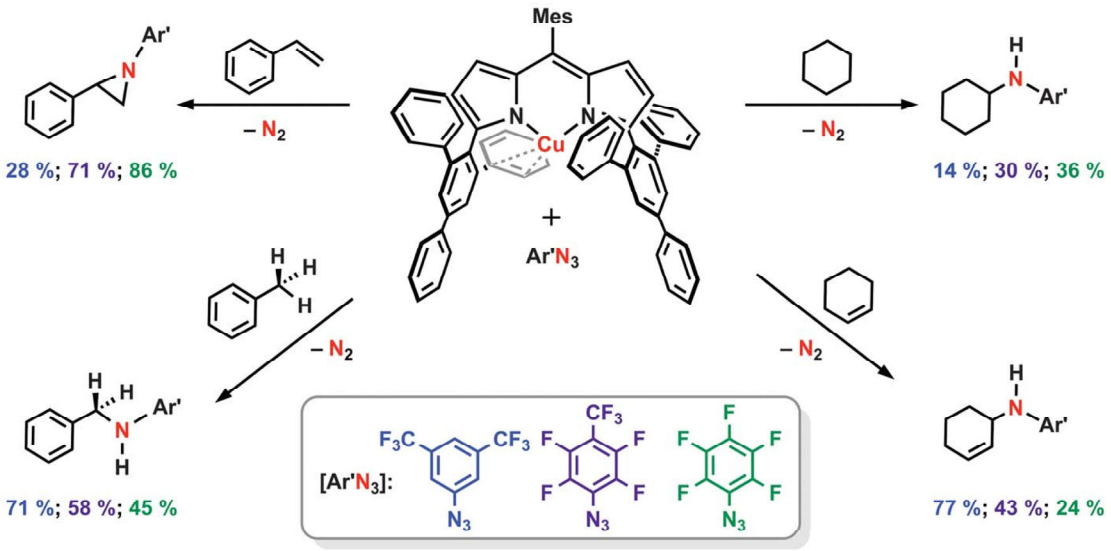
Mes
Cu
N
N
+
Ar'N3
Ar'
N
– N2
28 %; 71 %; 86 %
– N2
H
N
Ar'
14 %; 30 %; 36 %
H
H
H
– N2
H
H
N
Ar'
H
71 %; 58 %; 45 %
– N2
H
N
Ar'
77 %; 43 %; 24 %
[Ar'N3]:
F3C
CF3
N3
CF3
F
F
F
F
N3
F
F
F
F
F
F
N3

JACS
JOURNAL OF THE AMERICAN CHEMICAL SOCIETY
pubs.acs.org/JACS
Article

Reversible Scavenging of Dioxygen from Air by a Copper Complex

Kurtis M. Carsch,[‡] Andrei Iliescu,[‡] Ryan D. McGillicuddy, Jarad A. Mason, and Theodore A. Betley*

Cite This: *J. Am. Chem. Soc.* 2021, 143, 18346−18352
Read Online
ACCESS | Metrics & More | Article Recommendations | Supporting Information

ABSTRACT: We report that exposing the dipyrrin complex (^{EMind}L)Cu(N_3) to air affords rapid, quantitative uptake of O_2 in either solution or the solid-state to yield (^{EMind}L)Cu(O_2). The air and thermal stability of (^{EMind}L)Cu(O_2) is unparalleled in molecular copper-dioxygen coordination chemistry, attributable to the ligand flanking groups which preclude the $[Cu(O_2)]^{1+}$ core from degradation. Despite the apparent stability of (^{EMind}L)Cu-(O_2), dioxygen binding is reversible over multiple cycles with competitive solvent exchange, thermal cycling, and redox manipulations. Additionally, rapid, catalytic oxidation of 1,2-diphenylhydrazine to azoarene with the generation of hydrogen peroxide is observed, through the intermittency of an observable (^{EMind}L)Cu(H_2O_2) adduct. The design principles gleaned from this study can provide insight for the formation of new materials capable of reversible scavenging of O_2 from air under ambient conditions with low-coordinate Cu^I sorbents.

O_2 Manipulation through Solvent, Temperature, and Redox

J. Am. Chem. Soc. **2021**, *143*, 18346

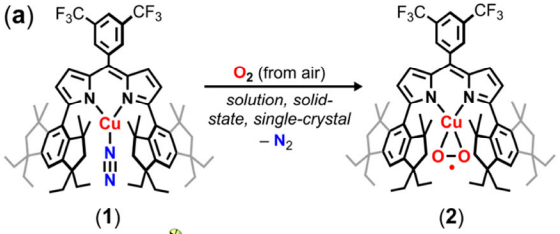
(a)
F3C
CF3
Cu
N
N
O2 (from air)
solution, solid-state, single-crystal
– N2
O
O
(1)
(2)
(b)
F
N
Cu
O
(c)
1.888(3)
1.885(3)
1.834(3)
1.824(3)
1.379(4)
Σ(Cu) = 360 °

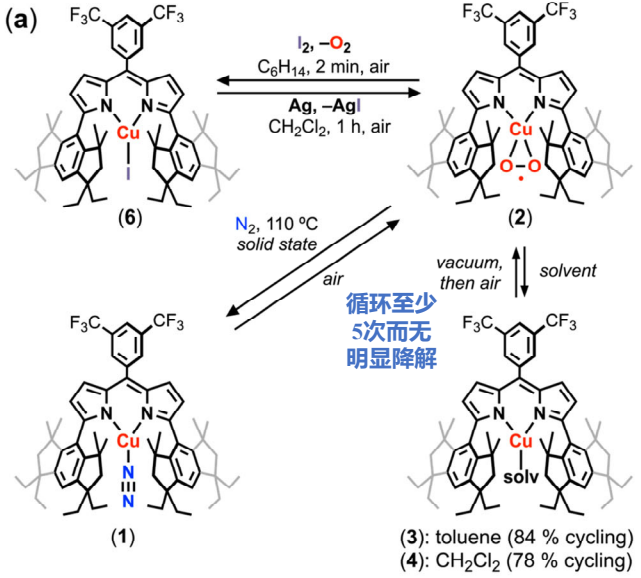
(a)
F3C
CF3
Cu
I
(6)
I2, –O2
C6H14, 2 min, air
Ag, –AgI
CH2Cl2, 1 h, air
O–O
(2)
N2, 110 ºC
solid state
air
vacuum,
then air
solvent
循环至少
5次而无
明显降解
N
N
(1)
solv
(3): toluene (84 % cycling)
(4): CH2Cl2 (78 % cycling)

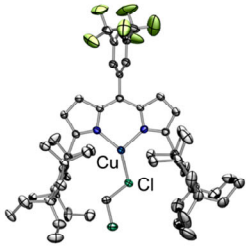
(b)
Cu
Cl
(4)

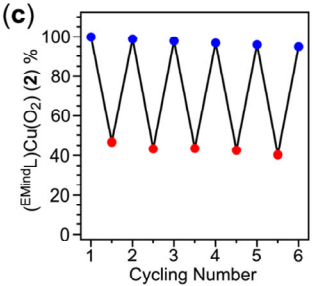
(c)
(EMind L)Cu(O2) (2) %
100
80
60
40
20
0
1
2
3
4
5
6
Cycling Number

实现了空气中可逆捕获氧气这一仿生过程，为开发下一代氧气分离技术提供了可能。

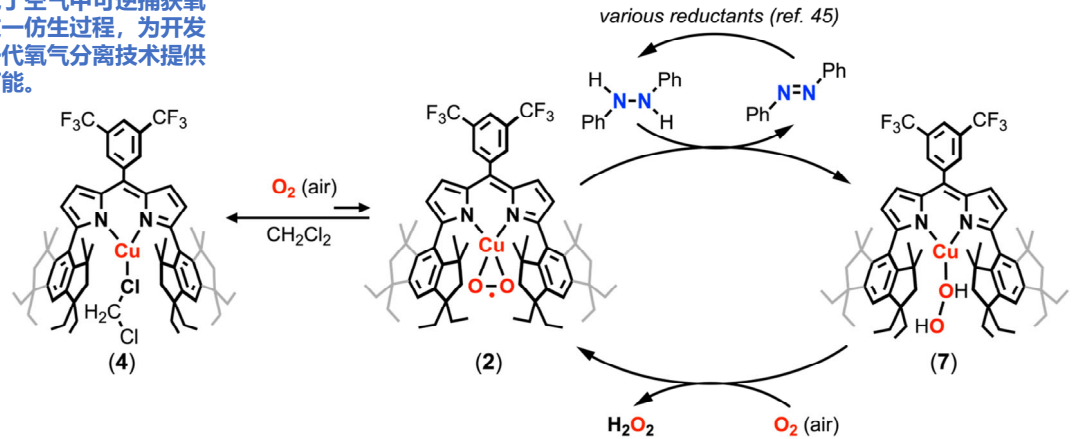

net reaction:

$$\mathbf{PhNHNHPh} + \mathbf{O_2\ (air)} \xrightarrow[\mathbf{CH_2Cl_2},\ 2\ h,\ RT,\ air]{\mathbf{2}\ (1\ mol\%)} \mathbf{PhNNPh\ (94\ \%)} + \mathbf{H_2O_2}$$

JACS
JOURNAL OF THE AMERICAN CHEMICAL SOCIETY
pubs.acs.org/JACS
Article

C–H Insertion from Isolable Copper Benzylidenes

Erika Amemiya, Shao-Liang Zheng, and Theodore A. Betley*

Cite This: *J. Am. Chem. Soc.* 2024, 146, 30653–30661 Read Online

ACCESS | Metrics & More | Article Recommendations | Supporting Information

ABSTRACT: Despite the utility of copper catalysts for the insertion of carbene moieties into C–H bonds, the copper carbene intermediate often invoked in these transformations has not been isolated. Herein, we describe the synthesis and structural characterization of a series of copper benzylidenes utilizing the sterically encumbered dipyrrin ligand (^{Em}L)H. These isolated copper carbenes demonstrate intramolecular insertion into the primary C(sp^3)–H bond of the ligand (^{Em}L)H and intermolecular insertion into ethereal and allylic C–H bonds. The copper carbenes isolated are best described as Cu(I) carbene adducts akin to canonical Fischer carbenes, given their diamagnetic ground state and electrophilic carbene reactivity. Furthermore, the insertion chemistry can be rendered catalytic utilizing a more sterically exposed dipyrrin ligand (^{ArF}L)H. The ability to isolate and observe stoichiometric C–H insertion and olefin cyclopropanation from well-characterized copper benzylidenes illuminates their viability as catalytic

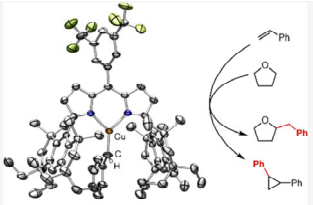

Isolated Copper(I) Benzylidene

J. Am. Chem. Soc. **2024**, *146*, 30653

Scheme 1. Synthesis of Copper Carbene Complexes

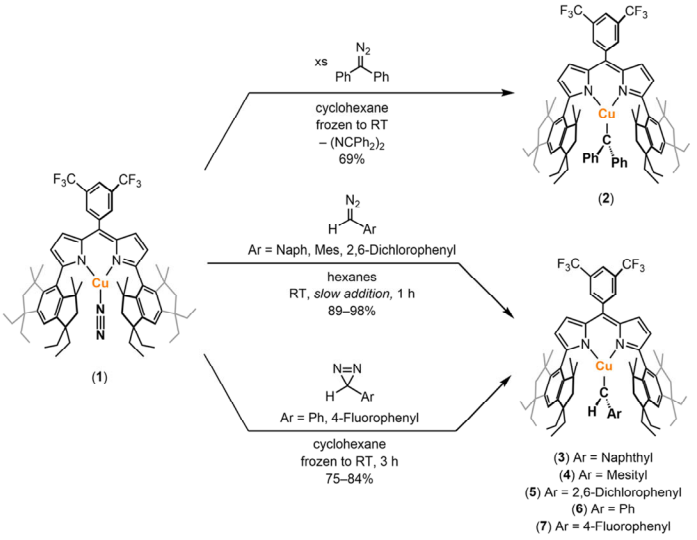

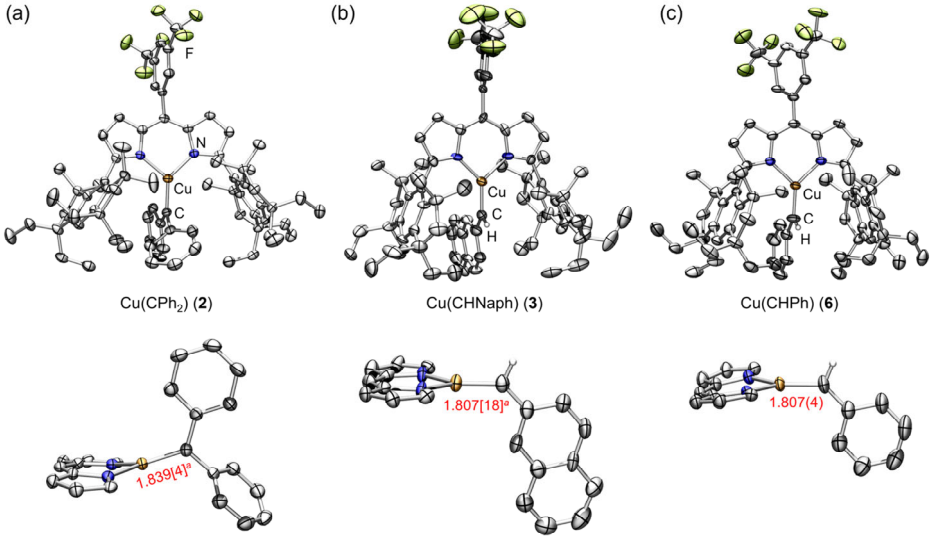

Fischer Cu卡宾：Cu–C(carbene) 键长（~1.807–1.897 Å）

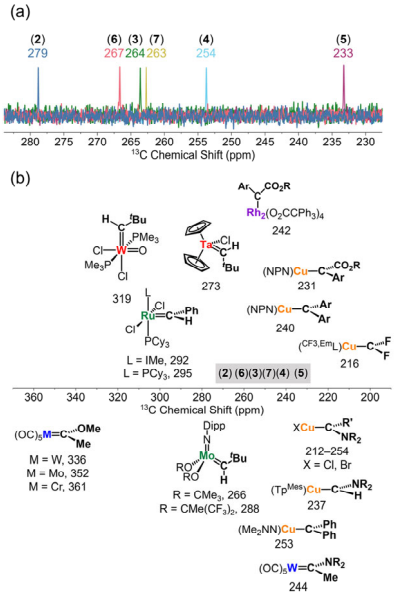

Figure 3. ^{13}C NMR chemical shifts of carbene carbon resonances for (a) copper carbenes reported in this work and (b) select Schrock alkylidenes (red), Fischer carbenes (blue), olefin metathesis catalysts (green), copper carbenes (orange), rhodium carbene (purple), and copper carbenes reported in this work (shaded gray).

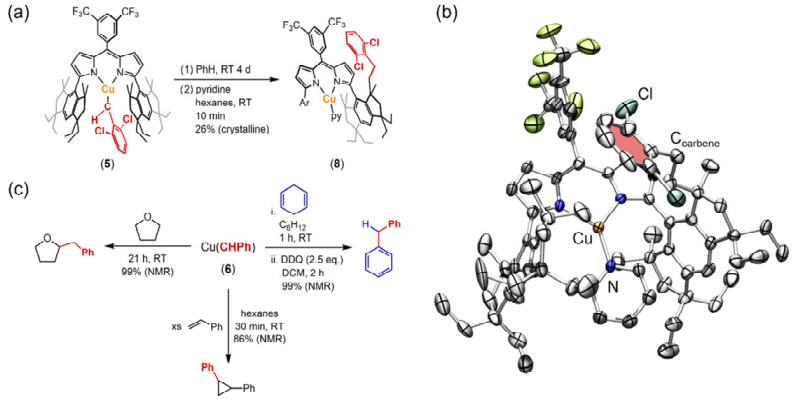

Figure 5. (a) Intramolecular carbene insertion into ligand, forming 8. (b) Solid-state structure of 8 with 50% ellipsoid probability. H atoms and solvent molecules omitted for clarity; carbene aryl group highlighted in red. (c) Stoichiometric intermolecular carbene insertion from isolated copper benzylidene.

JACS
JOURNAL OF THE AMERICAN CHEMICAL SOCIETY
pubs.acs.org/JACS
Article

Efficient C–H Amination Catalysis Using Nickel-Dipyrrin Complexes

Yuyang Dong, Ryan M. Clarke, Gerard J. Porter, and Theodore A. Betley*

Cite This: *J. Am. Chem. Soc.* 2020, 142, 10996–11005
Read Online

ACCESS | Metrics & More | Article Recommendations | Supporting Information

ABSTRACT: A dipyrrin-supported nickel catalyst (^{AdF}L)Ni(py) (^{AdF}L: 1,9-di(1-adamantyl)-5-perfluorophenyldipyrrin; py: pyridine) displays productive intramolecular C–H bond amination to afford N-heterocyclic products using aliphatic azide substrates. The catalytic amination conditions are mild, requiring 0.1–2 mol% catalyst loading and operational at room temperature. The scope of C–H bond substrates was explored and benzylic, tertiary, secondary, and primary C–H bonds are successfully aminated. The amination chemoselectivity was examined using substrates featuring multiple activatable C–H bonds. Uniformly, the catalyst showcases high chemoselectivity favoring C–H bonds with lower bond dissociation energy as well as a wide range of functional group tolerance (e.g., ethers, halides, thioetheres, esters, etc.). Sequential cyclization of substrates with ester groups could be achieved, providing facile preparation of an indolizidine framework commonly found in a variety of alkaloids. The amination cyclization reaction mechanism was examined employing nuclear magnetic resonance (NMR) spectroscopy to

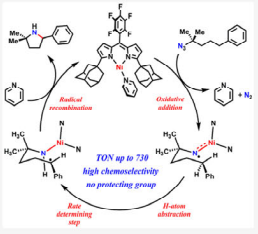

J. Am. Chem. Soc. **2020**, *142*, 10996

Scheme 1

Iminyl Formation

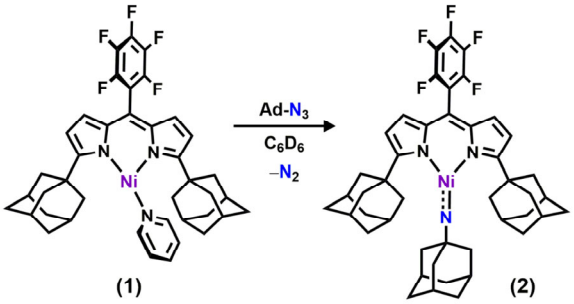

Catalytic Nitrile Formation

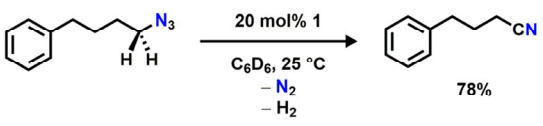

Table 1. Optimization of Amination Conditions[a]

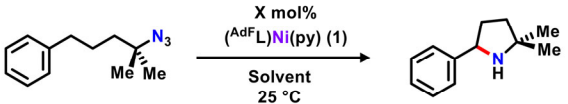

(3) (4)

Entry	Catalyst Loading (mol %)	Solvent	Time	Yield (%)[d]
1	10[b]	C_6D_6	10 min	>99
2	5[b]	C_6D_6	20 min	>99
3	2[b]	C_6D_6	40 min	97
4	1[b]	C_6D_6	90 min	96
5	0.1	C_6D_6	48 h	73
6	1[b]	Hexanes	90 min	95
7	1[b]	Et_2O	90 min	96
8	1[b]	(d_8-)Toluene[e]	90 min	95
9	1[b]	d_8-THF	90 min	94
10	10	d_6-DMSO	N/A[c]	0
11	10	d_4-Methanol	N/A[c]	0
12	10	DCM	N/A	0

单核金属络合物 (Ni)

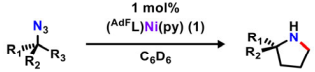

Entry	Substrate	Time (h)	Temperature (°C)	Product	Yield (%)
1	3	2	25	4	95
2	5	9[b]/2	25[b]/60	6[c]	65
3	7	6	60	8	88
4	9	24	60	10[c]	72
5	11[b]	48	80	12[c] · HCl	35

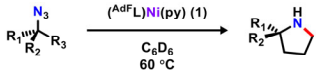

Entry	Substrate	Time (h)	Product	Yield (%)[b]
1	13	4	14	71
2	15	4	16	65
3	17	6	18	82
4	19	24	20	85
5	21	24	22a : 22b[c] 2 : 1	67

Table 4. Functional Group Tolerance[a]

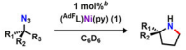

23 2 mol%, 25 °C, 2 hrs 92 %	**24** 2 mol%, 60 °C, 2 hrs 84 %	**25** 25 °C, 2 hrs 91 %	**26** 25 °C, 2 hrs 82 %	**27** 2 mol%, 60 °C, 2 hrs 75 %
28 2 mol%, 60 °C, 2 hrs 65 %	**29** 25 °C, 2 hrs 94 %	**30** 25 °C, 2 hrs 82 %	**31** 1) 60 °C, 2 hrs 2) K_2CO_3, MeOH, 10 hrs 66 %	
32 25 °C, 2 hrs 80 %	**33** 25 °C, 2 hrs 80 %	**34** 25 °C, 2 hrs 77 %	**35**[c] 10 mol%, 80 °C, 24 hrs no reaction	**36**[c] 10 mol%, 80 °C, 24 hrs no reaction
37 2 mol%, 60 °C, 2 hrs 76 %	**38** syn:anti > 99:1 25 °C, 2 hrs 73 %	**39** d.r. = 4.3 : 1 25 °C, 4 hrs 89 %	**40** 25 °C, 2 hrs 84 %	**41** 10 mol%, 80 °C, 24 hrs trace

[a]All yields noted are isolated yields. [b]Default catalyst loading (1 mol %) unless noted otherwise. [c]Functional groups detrimental to the catalysis are highlighted in green.

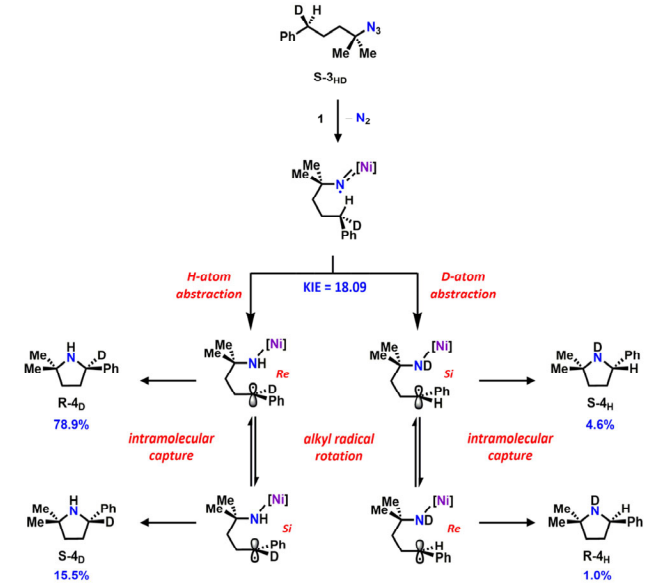

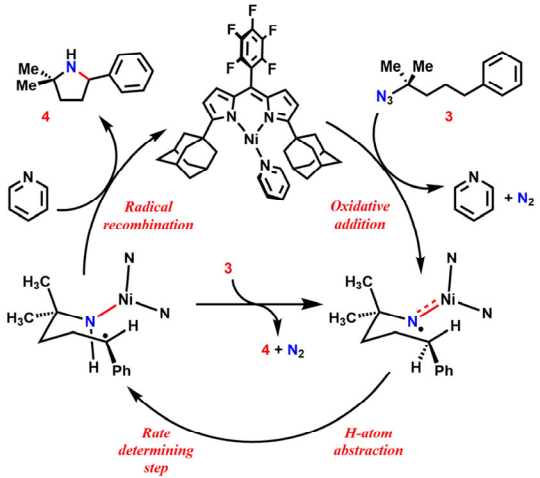

Figure 3. Proposed mechanism for C−H amination.

3_{D2}, KIE=31.9

JACS
JOURNAL OF THE AMERICAN CHEMICAL SOCIETY
pubs.acs.org/JACS
Article

Enantioselective C–H Amination Catalyzed by Nickel Iminyl Complexes Supported by Anionic Bisoxazoline (BOX) Ligands

Yuyang Dong, Colton J. Lund, Gerard J. Porter, Ryan M. Clarke, Shao-Liang Zheng, Thomas R. Cundari, and Theodore A. Betley*

Cite This: *J. Am. Chem. Soc.* 2021, 143, 817–829
Read Online

ACCESS | Metrics & More | Article Recommendations | Supporting Information

ABSTRACT: The trityl-substituted bisoxazoline (^{TrH}BOX) was prepared as a chiral analogue to a previously reported nickel dipyrrin system capable of ring-closing amination catalysis. Ligand metalation with divalent $NiI_2(py)_4$ followed by potassium graphite reduction afforded the monovalent (^{TrH}BOX)Ni(py) (**4**). Slow addition of 1.4 equiv of a benzene solution of 1-adamantylazide to **4** generated the tetrazido (^{TrH}BOX)Ni(κ^2-N_4Ad_2) (**5**) and terminal iminyl adduct (^{TrH}BOX)Ni(NAd) (**6**). Investigation of **6** via single-crystal X-ray

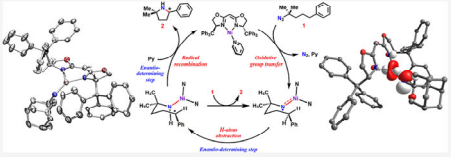

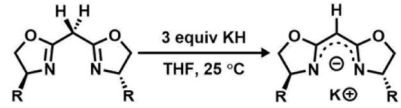
3 equiv KH
THF, 25 °C
1a, R = CPh3
1b, R = Ph
1c, R = tBu
2a, R = CPh3
2b, R = Ph
2c, R = tBu

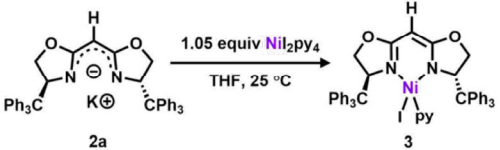
1.05 equiv NiI2py4
THF, 25 °C
2a
3

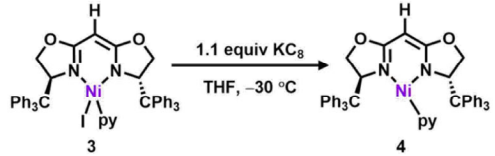
1.1 equiv KC8
THF, –30 °C
3
4

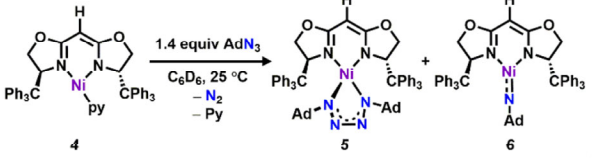
1.4 equiv AdN3
C6D6, 25 °C
– N2
– Py
4
5
6

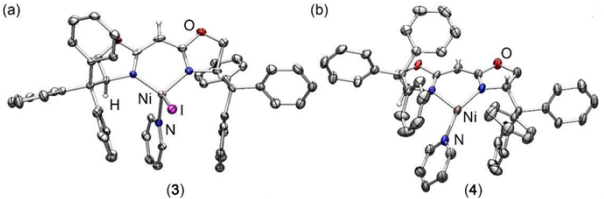
(a)
(b)
(3)
(4)

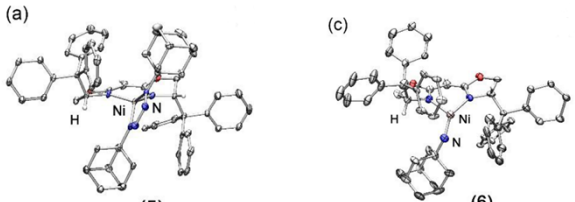
(a)
(c)
(5)
(6)

Scheme 5

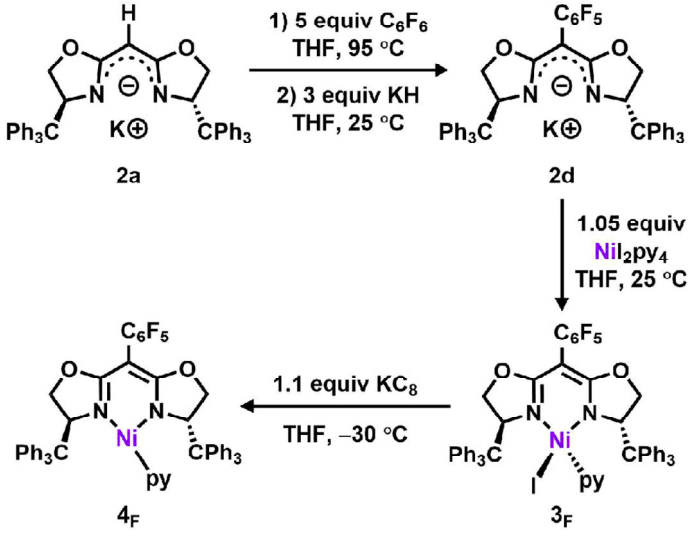
H
O
N
N
O
Ph3C
K⊕
CPh3
2a
1) 5 equiv C6F6
THF, 95 °C
2) 3 equiv KH
THF, 25 °C
C6F5
2d
1.05 equiv
NiI2py4
THF, 25 °C
1.1 equiv KC8
THF, –30 °C
Ni
py
I
4F
3F

Table 2. Substrate Scope[a]

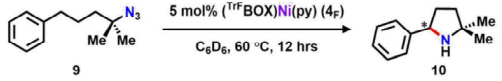

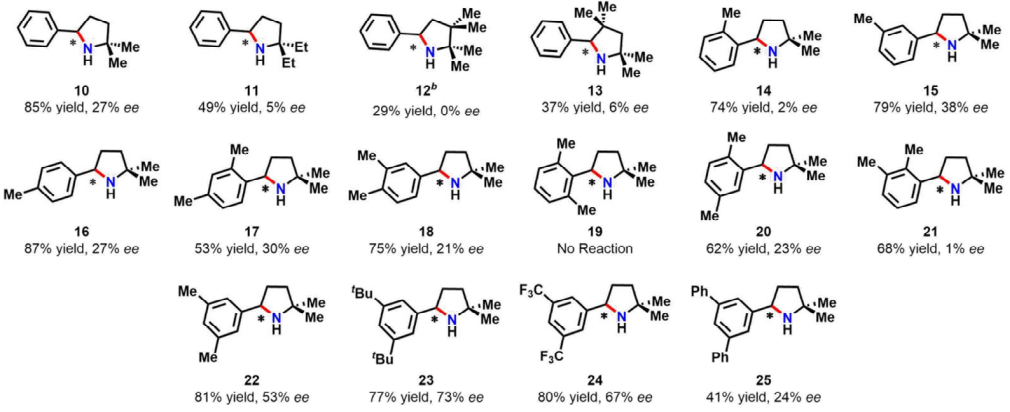

[a]Isolation yield. [b]50 mol % of catalyst was used due to the side product generated by carbocation rearrangement during the substrate preparation through S_N1 mechanism (see the SI).

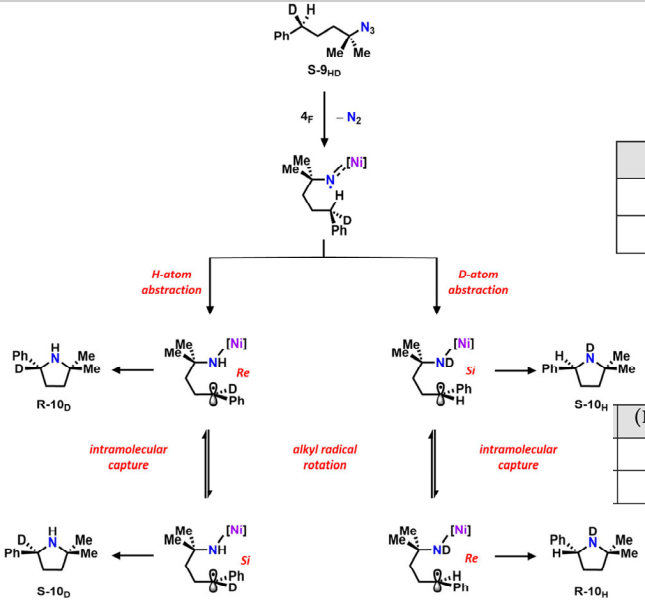

KIE = 1.35

Azide	S-10$_H$	R-10$_H$	S-10$_D$	R-10$_D$
S-9$_{HD}$	3.5%	1.7%	60.4%	34.4%
R-9$_{HD}$	23.2%	11.6%	49.9%	15.3%

(R-10$_D$+S-10$_D$)/ (R-10$_H$+S-10$_H$)	S-10$_H$/R-10$_H$	S-10$_D$/R-10$_D$
18.3:1	2.08	1.76
1.88:1	2.00	3.25

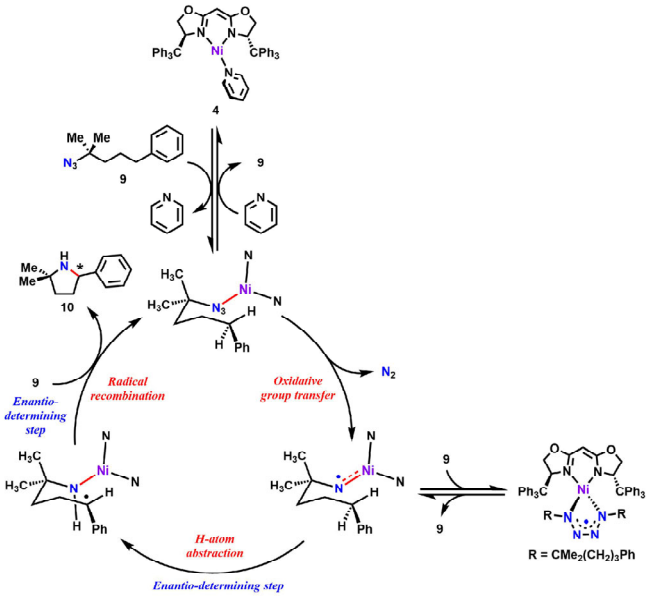

Table 3. Substrate Scope for Catalytic Enantioselective 2,5-Bis-Tertiary Pyrrolidine Synthesis[44]

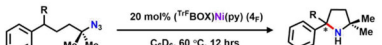

Substrate	Product
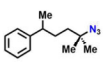 26	 27 50% yield, 53% *ee*
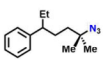 28	 29 78% yield, 76% *ee*
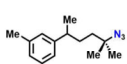 30	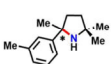 31 54% yield, 79% *ee*
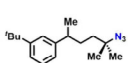 32	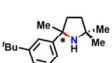 33 62% yield, 64% *ee*

Angewandte International Edition Chem

DOI: 10.1002/anie.201005198

Polynuclear Complexes

Synthesis and Redox Properties of Triiron Complexes Featuring Strong Fe–Fe Interactions**

*Qinliang Zhao and Theodore A. Betley**

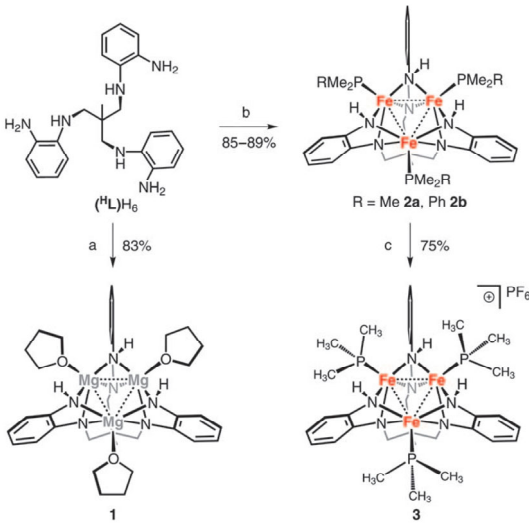

Scheme 1. Conditions: a) 3 equiv nBu$_2$Mg; b) 1.5 equiv [Fe$_2${N(SiMe$_3$)$_2$}$_4$], 3 equiv PMe$_2$R; c) Fc$^+$PF$_6^-$.

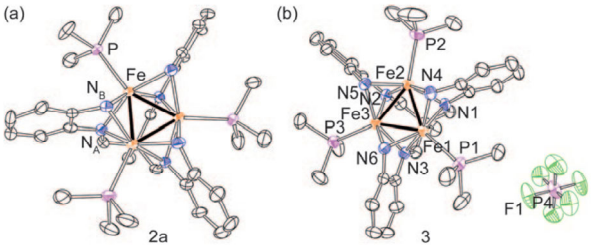

Figure 1. Solid-state molecular structures for a) **2a** and b) **3** with the thermal ellipsoids set at the 50% probability level (hydrogen atoms omitted for clarity; Fe orange, C black, N blue, P magenta, F green). Average bond lengths [Å] for **2a** (from 4 molecules in asymmetric unit): Fe–Fe 2.2995(19), Fe–N_A 1.984(8), Fe–N_B 2.024(8), Fe–P 2.324(4), N–C_{Ar} 1.411(12), C_{Ar}–C_{Ar} 1.392(14). Bond lengths [Å] for **3**: Fe1–Fe2 2.2499(4), Fe1–Fe3 2.2868(4), Fe2–Fe3 2.2863(5); average bond lengths: Fe–N1,2,3 2.001(2), Fe–N4,5,6 1.986(2), Fe–P 2.363(1), N–C_{Ar} 1.415(3), C_{Ar}–C_{Ar} 1.392(4).

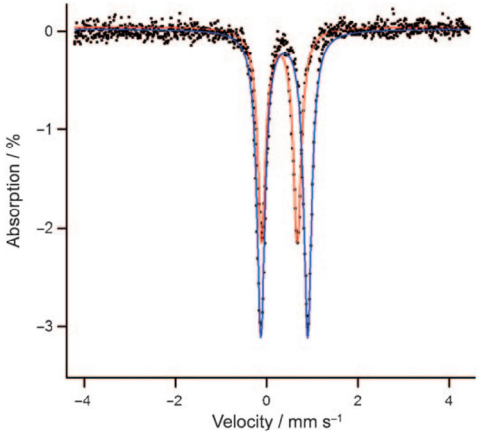

Figure 2. Zero-field ^{57}Fe Mössbauer spectra obtained at 77 K for **2a** represented by black dots and spectral fit as solid blue line (δ, $|\Delta E_Q|$ [mm s^{-1}]): 0.38, *1.03*; and for **3** represented by black dots and spectral fit as solid red line (δ, $|\Delta E_Q|$ [mm s^{-1}]): 0.28, *0.78*.

多核金属络合物：Fe, Cr, Ni, Mn, Cu, Co

仿生启发性：向自然学习

(1) 固氮：固氮酶中的铁钼辅因子是一个复杂的多核金属簇，能够在常温常压下将惰性的 N_2 转化为 NH_3。这是目前任何人造催化剂都无法比拟的。

(2) 光合作用：光合系统中的放氧中心是一个 Mn_4CaO_5 簇，通过四核锰中心的协同作用，高效、安全地催化水氧化生成氧气，这是地球上绝大多数生命的能量来源。

(3) 呼吸作用：细胞色素 C 氧化酶中含有双核铜中心和血红素铁中心，协同催化 O_2 的还原。